

# Design and Fabrication of a Piezoelectric Stack Actuator for Use in a Needle-Free Jet Injector

by

Randall Miller Briggs

Submitted to the Department of Mechanical Engineering  
in partial fulfillment of the requirements for the degree of

Master of Science in Mechanical Engineering

at the

MASSACHUSETTS INSTITUTE OF TECHNOLOGY

June 2018

© Massachusetts Institute of Technology 2018. All rights reserved.

**Signature redacted**

Author .....

Department of Mechanical Engineering

May 22, 2018

**Signature redacted**

Certified by .....

Ian W. Hunter

Hatsopoulos Professor of Mechanical Engineering

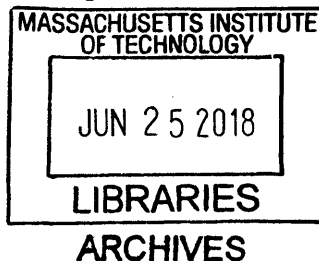
Thesis Supervisor

**Signature redacted**

Accepted by .....

Rohan Abeyaratne

Chairman, Department Committee on Graduate Students





# Design and Fabrication of a Piezoelectric Stack Actuator for Use in a Needle-Free Jet Injector

by

Randall Miller Briggs

Submitted to the Department of Mechanical Engineering  
on May 22, 2018, in partial fulfillment of the  
requirements for the degree of  
Master of Science in Mechanical Engineering

## Abstract

This thesis presents the design of a piezoelectric ceramic stack actuator for use with needle-free jet injection (NFJI) devices. While NFJI devices have been in use for over 60 years only recently have they been electronically actuated which allows for precise control of jet velocity, penetration depth, and injection volume. Most NFJI devices have been designed for fluids with a similar viscosity to water. Here we design an actuator for use with high viscosity fluids and non-newtonian fluids. The piezoelectric stack actuator presented in this work has been designed to deliver injection volumes of up to 30 microliters while pressurizing the fluid to over 40 MPa in order to achieve the necessary fluid velocities for injection. We have further presented all the methods used in order to fabricate functional lead zirconate titanate (PZT) piezoelectric ceramic discs. These discs are the basic building blocks for assembling a full stack actuator for NFJI.

Thesis Supervisor: Ian W. Hunter

Title: Hatsopoulos Professor of Mechanical Engineering



## Acknowledgments

I would like to thank Prof. Hunter first of all. He has created a truly unique environment in the BioInstrumentation Laboratory where students can feel completely free and encouraged to explore subject areas outside of their normal domain of expertise. This atmosphere has really helped me to get out of the mentality of only being a mechanical engineer. Instead, I have learned to not narrowly define myself and to be willing to learn necessary information from a wide variety of fields in order to tackle the difficult problems in science and engineering.

I would also like to thank all of my lab members in the BioInstrumentation Laboratory. They have provided essential guidance and many instances of advice and assistance with my work. My experience in the lab would have been quite empty without the help and friendship of all the awesome lab members.

I am so thankful to my parents for all their love and support over the years. I would especially like to thank my dad for how much he did and how hard he worked so that I could be at MIT and graduate. He always cared about our education so much and did everything in his power to give us the best education in the world. There is no way that I would be at MIT without him. I lost my dad during the course of this thesis work and it has been a very trying time. I know that he would be proud to see me completing my Masters Degree. I love you, dad. I can't wait to see you again.

I would like to especially thank my dear wife, Johanna. She has stood by me through some very difficult times in these past three years and she has been a constant source of support and comfort through all of the ups and downs of graduate life. Thank you, Johanna, for being willing to pass through this adventure together with me. You're really my best friend.

"But thanks be to God, who always leads us in triumph in the Christ and manifests the savor of the knowledge of Him through us in every place."

—2 Corinthians 2:14



# Contents

<b>1</b>	<b>Introduction</b>	<b>13</b>
1.1	The Purpose of this Thesis . . . . .	13
1.2	Background . . . . .	14
1.2.1	Past Work in Piezoelectric Actuators for NFJI . . . . .	14
<b>2</b>	<b>Design of the Piezoelectric Actuator</b>	<b>19</b>
2.1	Introduction to Piezoelectric Actuator Theory . . . . .	19
2.1.1	Piezoelectric Effect . . . . .	19
2.1.2	Poling of Piezoelectric Ceramics . . . . .	20
2.2	Design Parameters . . . . .	24
2.2.1	NFJI for High-Viscosity, Non-Newtonian Fluid Injection . . . . .	24
2.2.2	Detailed Design Parameters . . . . .	24
2.3	Choice of Piezoelectric Material . . . . .	25
2.3.1	Important Properties of Piezoelectric Materials . . . . .	25
2.4	Systematic Design of Piezoelectric Actuator . . . . .	29
2.4.1	Setting Other Design Parameters . . . . .	31
2.4.2	Calculation of Green Ceramic Dimensions . . . . .	33
2.4.3	Stack Dimensions . . . . .	35
2.4.4	Lost Volume . . . . .	36
2.4.5	Resonant Frequency . . . . .	37
2.4.6	Electrical Properties . . . . .	38
2.4.7	First Order Fluid Calculations . . . . .	40
2.4.8	Maximum Pressure Achieved . . . . .	41

2.5	Results of Design Process . . . . .	44
<b>3</b>	<b>Fabrication of Piezoelectric Actuator</b>	<b>47</b>
3.1	Overview of Steps . . . . .	47
3.2	Details of Fabrication Process . . . . .	48
3.2.1	PZT Powder . . . . .	48
3.2.2	Pressing . . . . .	49
3.2.3	Binder Burn Out . . . . .	49
3.2.4	Sintering . . . . .	51
3.2.5	Disc Slicing . . . . .	52
3.2.6	Polishing . . . . .	53
3.2.7	Poling . . . . .	54
<b>4</b>	<b>Experimental Analysis</b>	<b>59</b>
4.1	Method of Testing Individual Discs . . . . .	59
4.2	Results and Discussion . . . . .	61
<b>5</b>	<b>Conclusion</b>	<b>63</b>
5.1	Future Work . . . . .	63
5.1.1	High-Pressure Membrane Design . . . . .	63
5.1.2	High-Pressure Valve Design for Repeated Injections . . . . .	64
5.1.3	Binary Stochastic System Identification . . . . .	65
5.2	Summary of Conclusions . . . . .	65
<b>A</b>	<b>High Voltage Safety</b>	<b>67</b>



# List of Figures

1-1	Microjet device used for nanoliter injections. The transducer is a piezoelectric crystal element. Figure reproduced from [1]. . . . .	15
1-2	Piezoelectric microjet with a resistive-capacitive circuit which controls the expansion of the piezo actuator. Figure reproduced from [2]. . . . .	16
1-3	Mechanically amplified piezoelectric stack actuator in NFJI device. Figure reproduced from [3]. . . . .	17
2-1	Normal and Inverse Piezoelectric Effect. Figure reproduced from [4]. . . . .	20
2-2	Poling Process. Figure reproduced from [4]. . . . .	21
2-3	Structure of PZT Crystal above and below the Curie temperature, $T_C$ . Figure reproduced from [5]. . . . .	22
2-4	Rheology of HA. Figure reproduced from [6]. . . . .	25
2-5	Strain vs. Pressure for several piezoelectric materials available from APC. Material parameters taken from [7]. . . . .	27
2-6	High voltage stack actuator. Figure reproduced from [8]. . . . .	30
2-7	Full stack actuator assembly for NFJI. . . . .	34
2-8	Butterworth Van Dyke (BVD) equivalent circuit model for piezoelectric ceramics . . . . .	39
2-9	Impedance Bode plot for Butterworth Van Dyke (BVD) equivalent circuit model for piezoelectric ceramics. Figure reproduced from [9]. . . . .	39

2-10	Diagram showing the structural loop of the piezo actuator jet injector assembly. This diagram shows the equivalent stiffnesses of the structural members and the important deflections involved. The black arrows show the definition of positive values for $\Delta X_1$ and $\Delta X_2$ . The green arrows show the definition of positive forces in each spring equivalent element in the structural loop. . . . .	42
2-11	Photo of a typical PZT stack actuator after assembly. Image reproduced from [10]. . . . .	45
2-12	Diagram demonstrating the alternation of disc poling polarity and electrode voltage in a stack actuator. Figure reproduced from [9]. . . . .	45
3-1	PZT Spray-Dried Powder. Image reproduced from [11]. . . . .	49
3-2	Stainless steel punch and die for pressing. . . . .	50
3-3	Weighing out PZT powder for pressing. . . . .	51
3-4	Green ceramic rods after pressing. . . . .	52
3-5	Temperature profile for binder burn out step in furnace. The time axis is purposely left blank since the total time can vary. The total time of the process in our case was 20 hours. Figure reproduced from [12]. . . . .	53
3-6	SEM image of ceramic after the BBO step. Image taken by Jason Wang. . . . .	54
3-7	Sintering Enclosure. . . . .	55
3-8	Sintered Rods. . . . .	56
3-9	SEM image of sintered PZT ceramic. . . . .	56
3-10	Tank with mineral oil for slicing PZT ceramic rod. The sintered diamond saw blade is seen on the right side. The PZT ceramic rod is held in place in a custom machined collet on the left. The holding tank is made of clear acrylic in order to be able to see the process. . . . .	57
3-11	SEM image of polished PZT disc surface. . . . .	57

3-12	Image of the temperature-controlled mineral oil bath used for poling. The white block is made of PTFE and contains the metal plates with the PZT discs in the middle. The high voltage wires with silicone insulation are seen coming from the top to each side. . . . .	58
4-1	Three PZT discs tested. . . . .	59
4-2	Experimental setup for testing disc expansion and contraction. . . . .	60
4-3	Expansion test results. . . . .	62
5-1	High-pressure flexure-based piston seal. . . . .	63
5-2	Displacement field results of flexure-based seal FEA analysis. . . . .	64



# Chapter 1

## Introduction

### 1.1 The Purpose of this Thesis

#### **Provide a Background of Past Work**

It is important to understand the content of this thesis in the context of previous work. This thesis will give a brief overview of researchers who have employed actuators for needle-free jet injector (NFJI) devices made with piezoelectric ceramics.

#### **Introduce Basic Piezoelectric Actuator Theory**

In order to properly design a piezoelectric ceramic actuator for NFJI, it is crucial to understand key elements of piezoelectric actuator theory and material science. This thesis will provide a practical overview of how piezoelectric ceramics work, which material properties matter when designing a stack actuator for NFJI, and why certain attributes of piezoelectric ceramics make them an excellent choice for NFJI in certain applications.

#### **Describe the Relevance of Various Design Parameters for the Actuator**

While the majority of this thesis is meant to be a general guide to researchers who wish to make custom piezoelectric actuators for NFJI, this project was undertaken with a specific application of NFJI as the goal. In later sections, this thesis will

introduce the particular application of NFJI in more detail and will demonstrate how certain design parameters are constrained by the application.

Care will be taken to explain the physical meaning and implications of each design parameter so that the reader can set the design parameters themselves and use this work for many different types of applications.

### **Present a Systematic Method of Designing a Piezo Stack Actuator**

Based upon the design parameters, this thesis will present a method for systematically designing a piezoelectric stack actuator. I will discuss the important trade-offs involved when designing a stack actuator and will describe in detail how to sequentially create the design and then improve the design based on the design parameters.

### **Provide Detailed Instruction for the Fabrication of a Custom Piezo Stack Actuator**

This thesis will present detailed instructions for how to fabricate a custom piezoelectric ceramic actuator using lead zirconate titanate (PZT) powder. These instructions can be used both in a laboratory setting or, with some modification, can be scaled up in an industrial setting.

## **1.2 Background**

### **1.2.1 Past Work in Piezoelectric Actuators for NFJI**

Arora et al [1] used a piezoelectric ceramic actuator to make a pulsed microjet that would deliver many rapid injections of extremely small volumes. They hypothesized that bruising and pain caused by traditional NFJI systems was due to the deep penetration depth of the jet. Because their device was designed to provide rapid small volume injections of 2 to 15 nL the penetration depth was limited to about 200  $\mu\text{L}$ . The jet velocity of these small injections was still greater than 100 m/s. The piezoelectric ceramic actuator allowed them to deliver such small injections with a

relatively high velocity. Figure 1-1 shows a diagram of the device made by these researchers.

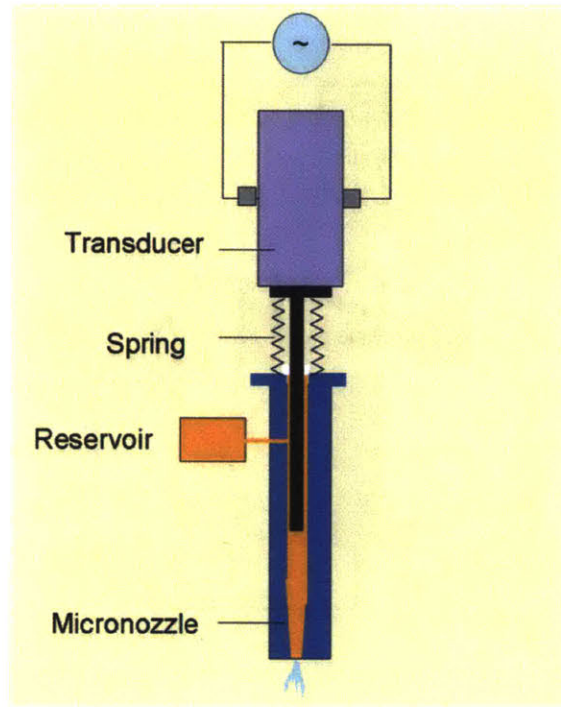


Figure 1-1: Microjet device used for nanoliter injections. The transducer is a piezo-electric crystal element. Figure reproduced from [1].

Stachowiak et al [2] used a piezoelectric ceramic actuator to control the jet velocity of a NFJI device. By adjusting the resistance of the electric path to charge the piezo actuator they were able to adjust the driving current and thus the driving velocity. Figure 1-2 shows a diagram of their experimental setup. The variable resistance circuit drives the piezo stack actuator from a fixed voltage source. The laser detector monitors the movement of the piston in order to determine the fluid velocity of the ejection.

Stachowiak et al [3] later demonstrated another NFJI device which used a piezo-electric stack actuator along with a mechanical amplifier which increased the output motion of the actuator. They were able to control the velocity of the jet in real time in order to control penetration depth. This was achieved by controlling the amount of time spend at a high velocity (for penetration) versus low velocity (for drug deliv-

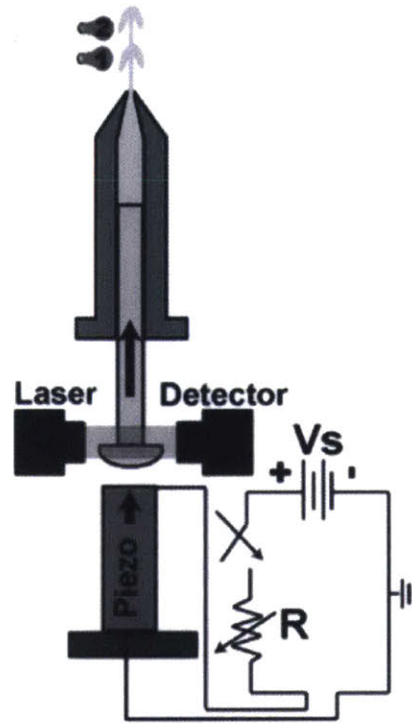


Figure 1-2: Piezoelectric microjet with a resistive-capacitive circuit which controls the expansion of the piezo actuator. Figure reproduced from [2].

ery). The typical ejection volumes during their experiments were 6 to 7  $\mu\text{L}$ . Figure 1-3 shows a diagram of this piezoelectric ceramic actuator along with the mechanical amplification stage.

In this thesis, we will demonstrate the design of a piezoelectric actuator for use in a NFJI device. This actuator is designed to provide both relatively large volume ejections (30  $\mu\text{L}$ ) and very high pressure in the fluid chamber (40 MPa). This device has been optimized for use with high viscosity and non-newtonian fluids which are difficult to eject with typical NFJI devices. Piezoelectric actuators are excellent for this purpose since they are able to pressurize the fluid chamber within microseconds and can quickly cause fluid flow with high pressure in order to induce shear thinning behavior.



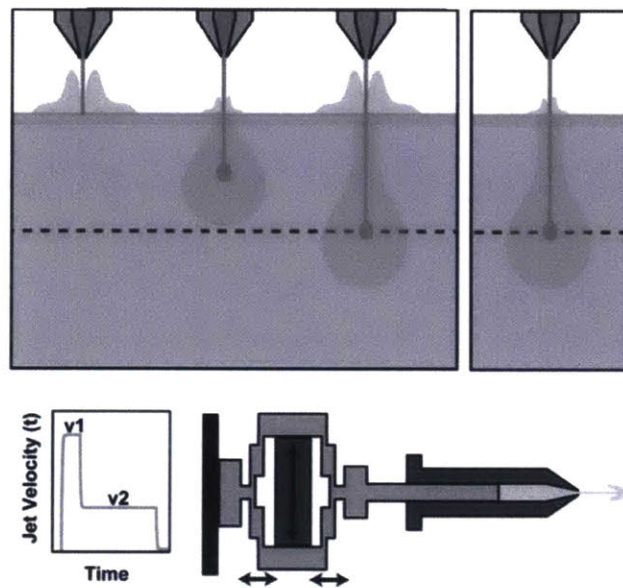


Figure 1-3: Mechanically amplified piezoelectric stack actuator in NFJI device. Figure reproduced from [3].



# Chapter 2

## Design of the Piezoelectric Actuator

### 2.1 Introduction to Piezoelectric Actuator Theory

In this section, I will describe the basic elements of piezoelectric theory that are important to understand when designing a piezo stack actuator for NFJI. There are many topics in piezoelectric material science that I will not cover since they are either irrelevant to this application or of second order importance.

#### 2.1.1 Piezoelectric Effect

The most critical feature of a piezoelectric material for use as an actuator is the expansion or contraction of the material when an electric field is applied in the same direction as the poling direction of the material. The poling direction is the direction in which all the electric dipoles in the material are aligned. This expansion under an applied electric field is actually called the inverse piezoelectric effect. Figure 2-1 shows the difference between the inverse piezoelectric effect and the normal or forward piezoelectric effect.

The "generator action" or normal piezoelectric effect is that the material will produce a large voltage between the opposite faces of the material when a mechanical stress is applied in the poling direction of the material. If the mechanical stress is squeezing the material in the poling direction, the voltage produced will be in the

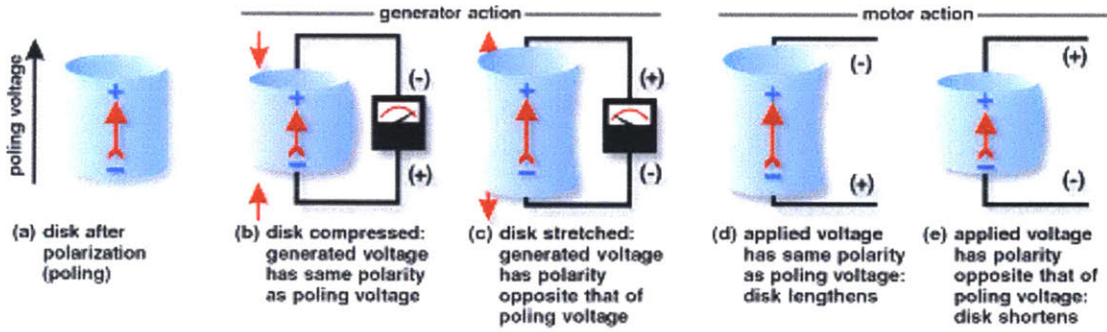


Figure 2-1: Normal and Inverse Piezoelectric Effect. Figure reproduced from [4].

same direction as the poling polarity. If the material is stretched parallel to the poling direction, this voltage will be in the opposite direction as the poling polarity. The poling polarity is shown in part (a) of Figure 2-1.

The "motor action" or inverse piezoelectric effect is that the material will expand or contract when an electric field is applied to the material. If the electric field is applied with the same polarity as the poling polarity, the material will expand in this direction (and shrink slightly in the perpendicular direction). If the electric field is applied with the opposite polarity of the poling polarity, the material will compress in this direction (and expand slightly in the perpendicular direction).

### 2.1.2 Poling of Piezoelectric Ceramics

We have mentioned that the poling polarity is determined by the direction of alignment of the electric dipoles in the material. In this section we will describe how dipole alignment is achieved. Polarization or "poling" is the process of using an applied electric field at high temperature to align the dipoles in a piezoelectric material.

#### Piezoelectric Ceramic Material Structure

All piezoelectric ceramics are made up of many small crystal domains that are randomly oriented when the ceramic is first made. Within each of these individual crystal domains the crystal structure is uniform and thus the crystal domain has a single dipole polarity direction. Figure 2-2 part (a) shows this state of the ceramic

material. These crystal domains are then aligned by applying a large (2-3 MV/m) external electric field as seen in part (b) of Figure 2-2. Poling is done at an elevated temperature which increases the mobility of the individual crystal domains. This elevated temperature drastically increases the rate of polarization. Once the external electric field is removed and the ceramic cools the crystal domains remain largely oriented in the same direction. This final state of alignment is called the remnant polarization and can be seen in part (c) in Figure 2-2. The material will keep the majority of this remnant polarization essentially indefinitely, unless it is lost due to mechanical stress, high temperature exposure, or a high electric field in the opposite direction of the poling.

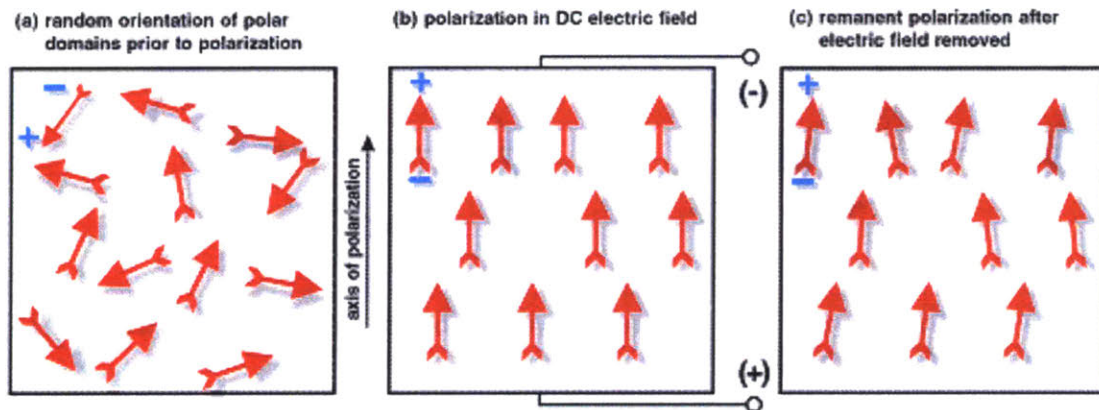


Figure 2-2: Poling Process. Figure reproduced from [4].

## Curie Temperature

As mentioned previously, the poling process is performed at a high temperature in order to drastically speed up the process. The target temperature for this process is a few degrees Celsius lower than the Curie temperature for the particular piezo material. The Curie temperature is the temperature that marks the transition between two crystal structures of the material.

Above the Curie temperature, the crystal structure of the material loses its dipole moment. Without the dipole moment, the crystal domains cannot be oriented using an electric field. Below the Curie temperature, the crystal structure obtains an asym-

metry that produces the electric dipole moment. This is why it is crucial that poling be performed at a temperature slightly lower than the Curie temperature. Figure 2-3 shows how the structure of lead zirconate titanate (PZT) crystal changes above and below the Curie temperature.

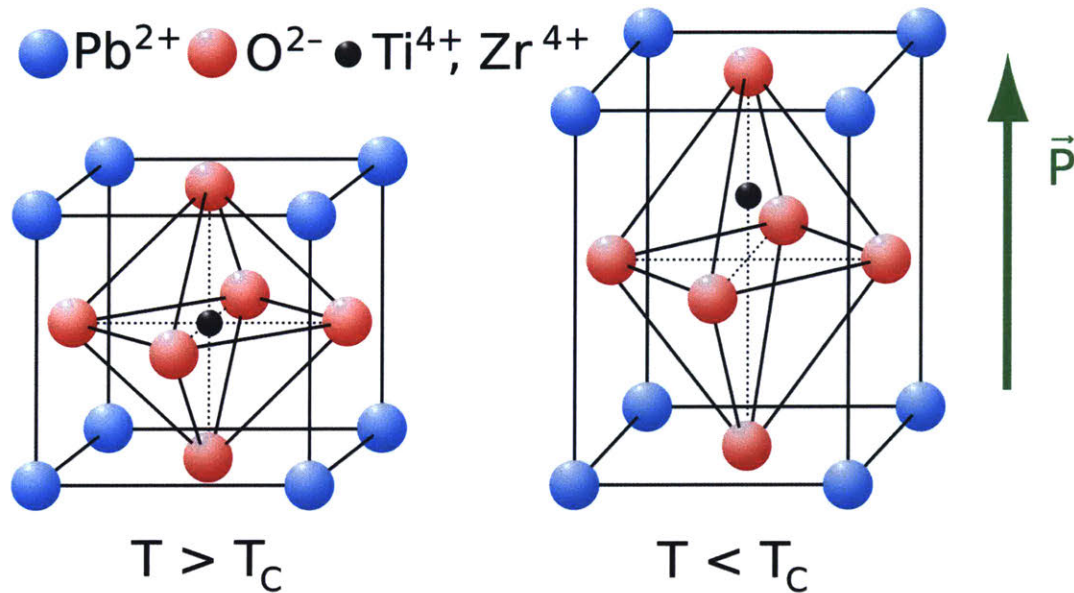


Figure 2-3: Structure of PZT Crystal above and below the Curie temperature,  $T_C$ . Figure reproduced from [5].

### Causes of Depolarization

It is possible for a material to lose its polarization after the poling process has been completed. It is important to be aware of the various conditions that can cause the material to depolarize. Depolarization will reduce the effectiveness of the piezo actuator and could render the actuator useless. Below is a partial list of the common conditions that can lead to depolarization:

1. **Thermal Depolarization** - Heating a piezo ceramic material up to the Curie temperature will certainly cause depolarization. It is recommended to operate at a significantly lower temperature. The recommended upper operating temperature is approximately half-way between 0 °C and the Curie temperature of the material [7, p. 23].

2. **Mechanical Depolarization** - A very high mechanical stress applied to a piezo ceramic can disturb the orientation of the crystal domains and thus cause depolarization. The susceptibility to this phenomenon varies with different materials [7, p. 23].
  
3. **Pyroelectric Depolarization** - Even if the temperature of the material stays below the upper recommended operating temperature, rapid temperature swings can still cause depolarization. This is because rapid temperature fluctuations can actually generate high voltages in piezo ceramics which cause electrical depolarization. The strength of this effect also varies with different materials [7, p. 23].
  
4. **Electrical Depolarization** - Applying a strong electric field in the opposite direction of the poling polarity will cause depolarization in a piezo ceramic material. The degree of depolarization will depend on the exposure time, the temperature, the type of material, and other factors. In general any electric field in the range of 200 to 500 kV/m or greater applied in this direction will cause depolarization to some degree [7, p. 22].

### **Asymmetric Actuation**

Once a piezoelectric material has been polarized through the poling process, it can be actuated using an applied electric field. While a high electric field applied in the opposite direction of the poling polarity will cause depolarization, a high electric field applied in the same direction as the poling polarity will tend to reinforce the polarization of the material. Because of this effect, there is a significant asymmetry in the electric field that can be applied to the material. It follows that the material can be expanded much more than it can be contracted under an applied electric field. This feature will be important as we design our stack actuator.

## 2.2 Design Parameters

### 2.2.1 NFJI for High-Viscosity, Non-Newtonian Fluid Injection

This thesis is focused on designing a piezoelectric stack actuator that could be used to deliver small volumes (e.g. 10 to 30  $\mu\text{L}$ ) of fluid of variable viscosity to the upper dermis. A good example of such a high viscosity fluid is hyaluronic acid (HA) which also exhibits non-newtonian shear thinning behavior. We will use HA as an example high viscosity fluid to be delivered for this thesis. This specific application of the device gives us certain design parameters that we will use as a guide in designing the actuator.

### 2.2.2 Detailed Design Parameters

#### High Ejection Pressure

Hyaluronic acid (HA) is a non-newtonian fluid that can have a large range of dynamic viscosities at different shear rates. Figure 2-4 shows the typical relationship between shear rate and viscosity for HA

Based on experimental results within the BioInstrumentation lab, approximately 20 MPa has been found to be the required pressure to achieve a jet velocity which penetrates deep enough into porcine tissue. This required jet velocity is approximately 150 to 200 m/s.

#### Injection Volume

The required volume for each injection is approximately 10  $\mu\text{L}$ . In order to be conservative and protect against unexpected sources of lost injection volume, we will set this design parameter to be 30  $\mu\text{L}$ . This will allow us to deliver a full range of ejection volumes from 30  $\mu\text{L}$  down to 10  $\mu\text{L}$  and below.



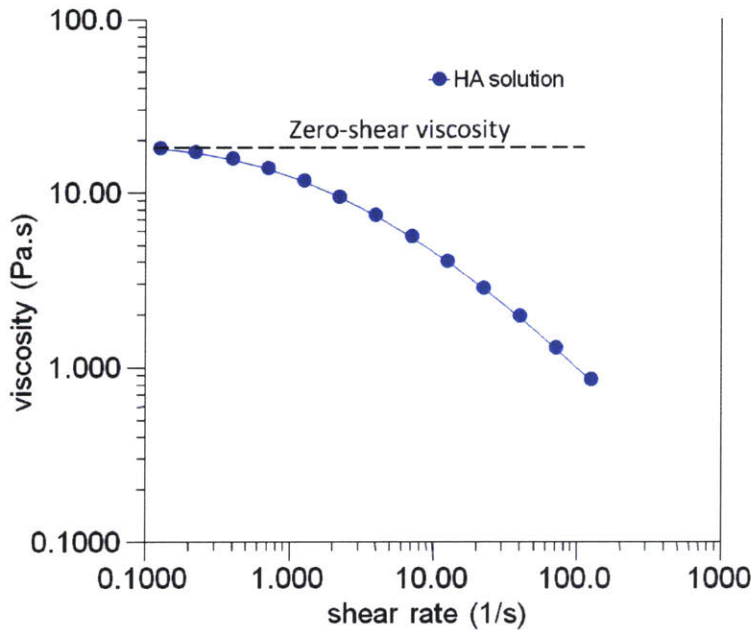


Figure 2-4: Rheology of HA. Figure reproduced from [6].

## 2.3 Choice of Piezoelectric Material

### 2.3.1 Important Properties of Piezoelectric Materials

One critical value that we are interested in for our application is the maximum pressure that can be exerted by a piezo actuator since this is directly related to the ejection pressure. Surprisingly, this is determined by only three material properties:  $d_{33}$  - the piezoelectric charge constant in the poling direction,  $E_{33}$  - the elastic modulus of the material in the poling direction, and  $E_{max}$  - the maximum electric field that the material can sustain before dielectric breakdown occurs. The maximum achievable pressure is simply the product of these three parameters as seen in Equation 2.1 below:

$$P_{max} = d_{33} \cdot E_{33} \cdot E_{max} . \quad (2.1)$$

This maximum pressure is achieved when the maximum electric field is applied to a piece of piezoelectric material that is constrained from expanding. As the piezoelectric piece is allowed to expand, the pressure drops linearly until the piezo piece

reaches its new equilibrium length. This effect is seen in Figure 2-5 for several different piezoelectric materials. The maximum pressure that can be achieved by the piezoelectric element is also called the blocking pressure. In Figure 2-5 the blocking pressure is the intersection of the strain vs. pressure line with the horizontal axis.

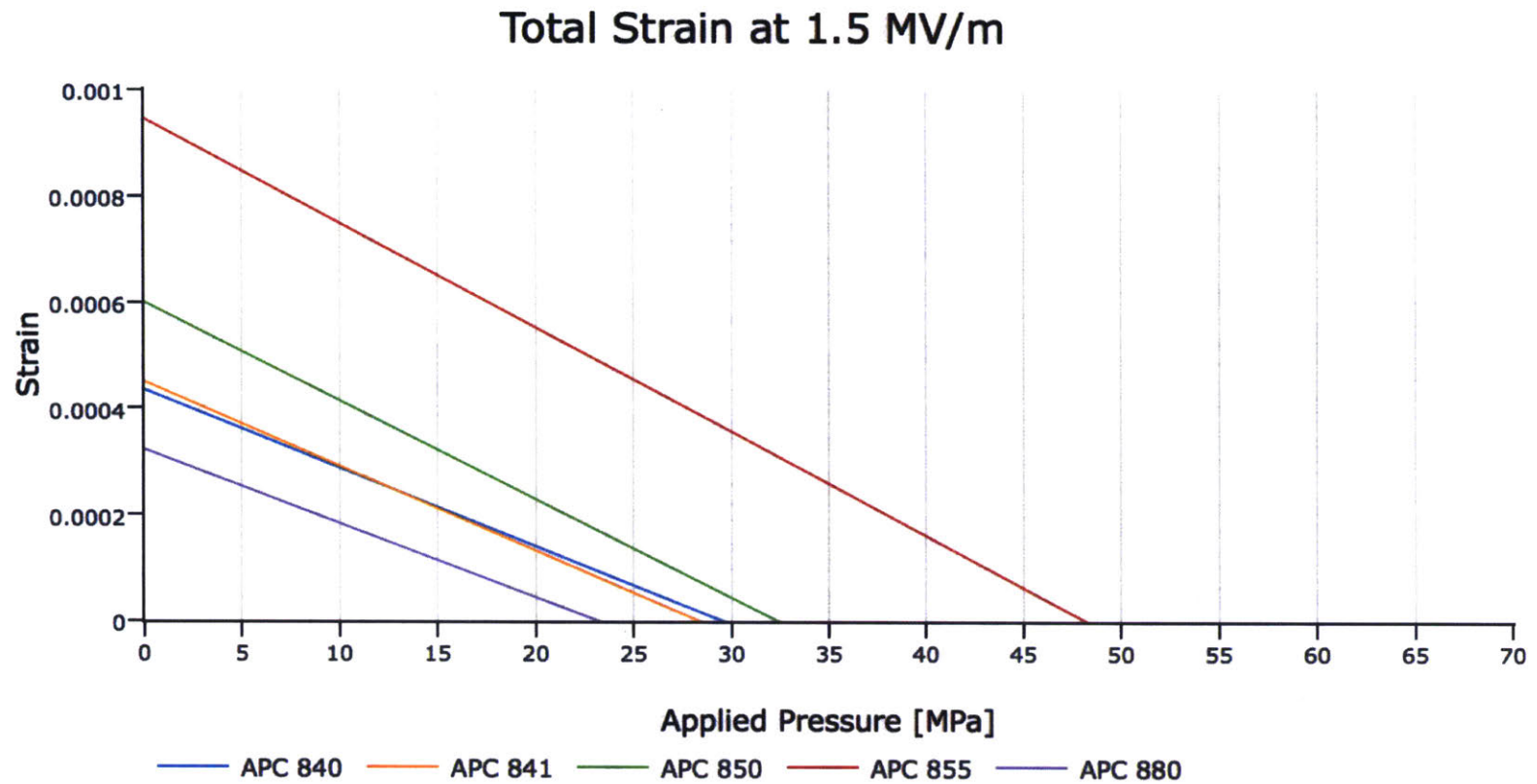


Figure 2-5: Strain vs. Pressure for several piezoelectric materials available from APC. Material parameters taken from [7].

The equation for the strain,  $\epsilon$ , of the piezoelectric material plotted in Figure 2-5 is

$$\epsilon = d_{33} \cdot E_{max} - \frac{P_{applied}}{E_{33}} . \quad (2.2)$$

As can be seen from this equation, the piezoelectric charge constant,  $d_{33}$ , multiplied by the maximum electric field,  $E_{33}$ , sets the maximum strain for the piezo piece under no load. As the piezo piece is compressed by the applied pressure,  $P_{applied}$ , it shrinks until finally reaching its original length when the strain equals zero at the horizontal axis.

The blocking pressure alone is not the only important parameter to look at when choosing a piezoelectric material. If the material has a very high stiffness,  $E_{33}$ , and a relatively low piezoelectric charge constant,  $d_{33}$ , it is possible for the material to have a high blocking pressure with a low maximum strain value. For the purpose of ejecting a fluid, this means that the actuator will be able to exert a very high pressure to the fluid chamber but will eject only a very small volume of fluid. In order to eject a larger volume of fluid in this case, it would be necessary to increase the length of the actuator considerably. This lengthening is needed so that the small value of maximum strain multiplied by the original length equals the required change in length, or stroke of the piston. This basic formula is

$$\Delta L = \epsilon \cdot L_{original} . \quad (2.3)$$

The ejected volume,  $V_{ejected}$ , is equal to the area of the piston,  $A_{piston}$  multiplied by the change in length of the actuator,  $\Delta L$ , as

$$V_{ejected} = A_{piston} \cdot \Delta L . \quad (2.4)$$

In order to choose a piezoelectric material for use with NFJI it is necessary to decide upon the minimum pressure at which the jet velocity is still sufficiently high for injection to take place. We have already determined that 20 MPa is necessary to achieve the desired ejection velocity, but since our fluid is non-Newtonian, the

pressure needed to maintain this jet velocity should decrease once the fluid starts to flow. Thus, we will somewhat arbitrarily set the minimum pressure for injection at 10 MPa. We will assume that the volume ejected is only useful if ejected above or equal to this minimum pressure. Any fluid that is ejected below this pressure is assumed to have a velocity too low to penetrate the tissue.

This new requirement of a minimum ejection pressure helps us to further refine our selection process. Our process has three key steps:

1. For every material, calculate the blocking pressure and the maximum strain.
2. Plot strain versus applied pressure.
3. At the minimum pressure needed for injection choose the material that has the highest strain at this point. As long as this material also has a sufficiently high blocking pressure for the particular application, this is most likely the best choice.<sup>1</sup>

We can see from Figure 2-5 that APC material 855 has the highest strain at every pressure and in this case is the clear winner. All the materials on this plot are made by APC and are different variants of lead zirconate titanate (PZT).

## 2.4 Systematic Design of Piezoelectric Actuator

### Stack Actuator Design

This thesis is focused on the design of a piezoelectric stack actuator for use with NFJI. There are two primary types of piezoelectric stack actuators: high voltage stack actuators and low voltage stack actuators. High voltage stack actuators consist of individual piezoelectric ceramic discs which are stacked on top of each other with thin, metal electrodes in between each disc. Figure 2-6 shows the structure of a typical high voltage stack actuator. Low voltage stack actuators are made with a continuous,

---

<sup>1</sup>The reader should be aware that there could be a number of other important considerations when choosing a material such as maximum operating temperature, number of lifetime cycles, cost, manufacturability, density, brittleness, etc.

very thin strip of piezoelectric material on top of a very thin strip of metal. This tape is then folded back and forth on top of itself in order to form the stack actuator. High voltage stack actuators normally require about 1000 V to operate at full stroke. Low voltage stack actuators normally require about 100 V to operate at full stroke. In general, low voltage actuators have much higher capacitance than high voltage stack actuators and thus cannot normally be actuated as fast as high voltage stack actuators and require higher currents.

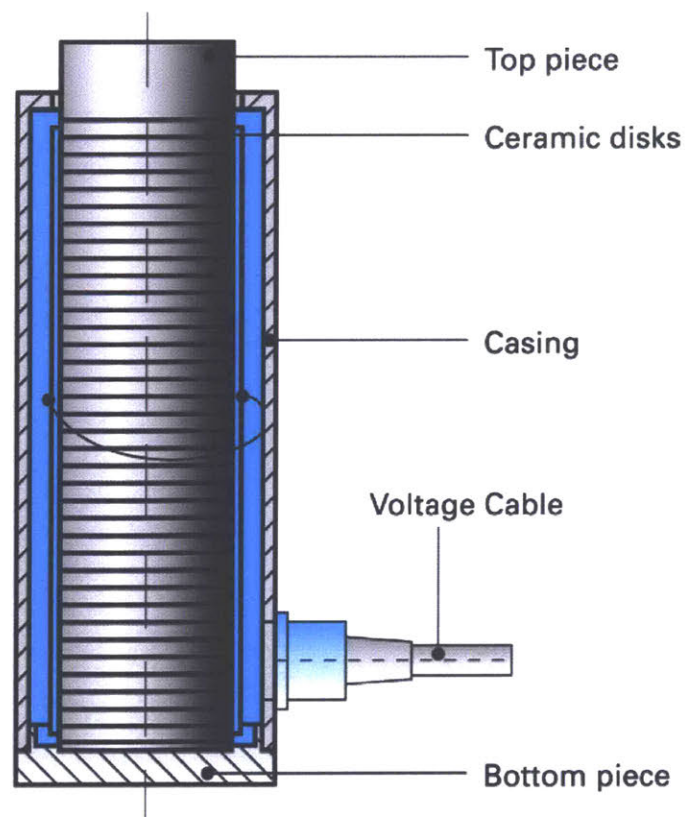


Figure 2-6: High voltage stack actuator. Figure reproduced from [8].

The primary reason we chose to fabricate a high voltage stack actuator is because of the relative ease of manufacturing individual piezoelectric ceramic discs rather than forming the thin tape necessary for a low voltage stack actuator. The relatively low capacitance of the high voltage stack actuator will also make it easier to provide the necessary driving currents in a small device.

### 2.4.1 Setting Other Design Parameters

We will now begin the design process by setting all the necessary parameters:

- $V_{inj}$  - The desired injection volume. We previously set this parameter to 30  $\mu\text{L}$ .
- $V_{fluid}$  - The total volume of fluid contained in the ejection chamber. This value will be important since the fluid itself will compress during ejection. The larger the volume of fluid in the ejection chamber, the lower the effective stiffness of the fluid becomes. We will set this to be 0.5 mL based on what is a reasonable fluid thickness (the thickness of the disc of fluid in the fluid ejection chamber). The fluid thickness in the fluid ejection chamber should be at least 10 times greater than the jet diameter so that the fluid dynamics are dominated by the high velocity jet and not by the viscous drag encountered by the fluid moving horizontally in the fluid ejection chamber.
- $G_{fluid}$  - The bulk modulus of the fluid. It was difficult to find an accurate value for HA so instead we used the average of the values for water and for glycerin. Water has a bulk modulus of 2.15 GPa and glycerin has a bulk modulus of 4.35 GPa. The average value which we used to represent the likely value of HA is 3.25 GPa. The bulk modulus will be used to calculate the ejection volume lost due to the compression of the fluid itself.
- $d_{33}$  - The piezoelectric charge constant. This is the piezoelectric charge constant for APC material 855, which we chose for our application. For the 855 material this value is  $630 \times 10^{-12}$  m/V.
- $E_{33}$  - The elastic modulus of the piezoelectric material in the direction of poling. For the 855 material this value is  $5.1 \times 10^{10}$  Pa.
- $E_{max}$  - The maximum electric field that can be withstood by the piezoelectric material. For PZT, the maximum electric field the material can withstand before experiencing dielectric breakdown is around 2 MV/m. We will avoid this limit and instead set this value to 1.5 MV/m in order to leave a margin of safety.

- $P_{min}$  - The minimum pressure required to sustain injection velocity. We will only count the volume of fluid ejected above this pressure. We have set this minimum pressure to be 10 MPa
- $E_{max}$  - The maximum electric field that will be applied to the piezoelectric material. It is important to remember that this electric field will only be applied to the piezoelectric material with the same polarity as the poling polarity. We have set this maximum electric field to be 1.5 MV/m.
- $V_{max}$  - The maximum voltage applied to the piezoelectric material. This value is largely determined by the driving electronics that we will use to control the voltage on the piezo stack actuator. The power electronics that we chose to drive the piezo stack actuator have a maximum voltage rating of 1200 V. We will plan on using 1000 V on our stack actuator in order to leave a margin of safety. As we mentioned earlier it is common for so called high voltage stack actuators to have a maximum applied voltage of about 1000 V.
- $D_{stack}$  - The diameter of the stack actuator. This is the diameter of the discs that are used to make the stack actuator. It is not the outer diameter of the steel case that forms the outside of the stack actuator unit. Since we hope for this device to be hand-held in the future, we realized that this diameter could be no more than approximately 45 mm. This parameter causes many changes in later calculations as we will see shortly. In summary, increasing the stack diameter will increase the length of the stack actuator (in order to preserve ejected volume), will increase the time required for the stack to fully extend when a step increase in voltage is applied, and will increase the ejected volume lost due to the elongation of the outer steel case. This value had to be optimized by hand while balancing all of these trade-offs. We settled for a value of 30 mm. We will explain this process in more detail in the sections to follow.
- $D_{piston}$  - The diameter of the piston driving the fluid. As seen in Figure 2-7 the diameter of the piston must necessarily be slightly smaller than the diameter



of the piezo stack itself since the preloading element will need to press down on the top of the stack below the piston head. We must make the piston slightly smaller in order to produce this surface for the preloading element to seat against. We will assume that a seating edge of 0.5 mm is sufficient based on the typical geometry of preloading elements such as Belville washers. So the piston diameter is 1 mm less than the stack diameter, or 29 mm.

- $A_{piston}$  - The area of the piston head driving the fluid. This is simply based on the diameter of the piston. This area is  $6.605 \times 10^{-4} \text{ m}^2$ .
- $t_{fluid}$  - The thickness of the disc of fluid in the ejection chamber. This value will be important for calculating the effective stiffness of the fluid in the structural loop. This value is simply the volume of the fluid divided by the area of the piston. It is equal to 0.757 mm.

## 2.4.2 Calculation of Green Ceramic Dimensions

The first practical calculation that we will need is the dimension of the "green" or unfired ceramic. The geometry of the stack actuator that we set as a parameter is describing the final, fired ceramic pieces. The ceramic will first be formed in larger dimensions and will shrink considerably in the process of firing.

We know from the literature (cite:APC blog) that the density of the pressed green ceramic will only be 60% of the density of the final ceramic pieces. This corresponds to an increase of density by a factor of 1.667:

$$\Delta_{density} = 1.667. \tag{2.5}$$

If the density of the ceramic increases by this much, then the volume will decrease by a corresponding amount. Linear dimensions of the ceramic piece will change by a factor of the cube root of the change in volume.  $\Delta_{lindim}$  is the factor of change in linear dimensions:

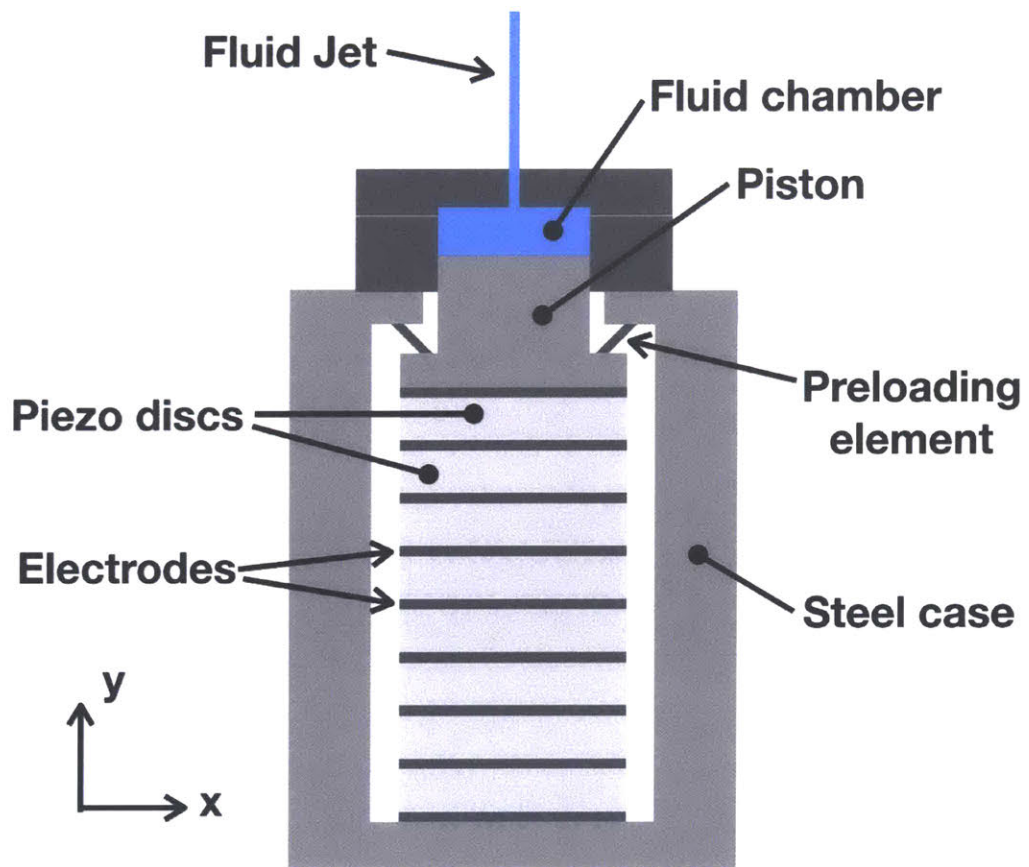


Figure 2-7: Full stack actuator assembly for NFJI.

$$\Delta_{lindim} = \sqrt[3]{\frac{1}{\Delta_{density}}} . \quad (2.6)$$

The value of  $\Delta_{lindim}$  is equal to 0.843. Multiplying the reciprocal of this value by the stack diameter will give us the necessary diameter of the green ceramic,

$$D_{green} = \frac{1}{\Delta_{lindim}} \times D_{stack} = 35.57 \text{ mm} . \quad (2.7)$$

### 2.4.3 Stack Dimensions

In this section we will calculate the overall stack actuator dimensions based on the parameters set earlier.

We first calculate the stroke of the piston (occurring above the minimum pressure) that will be required to eject the desired fluid volume,

$$Stroke_{pressure} = \frac{V_{inj}}{A_{piston}} = 45.42 \text{ } \mu\text{m} . \quad (2.8)$$

Next we will calculate the thickness of the piezoelectric ceramic discs,  $t_{disc}$ . This is simply determined by the maximum electric field and the maximum voltage set earlier,

$$t_{disc} = \frac{V_{inj}}{E_{max}} = 0.667 \text{ mm} . \quad (2.9)$$

We will set the thickness of electrode material,  $t_{electrode}$ , to be 0.1 mm. This is an approximate estimate of the thickness of material that will allow for plenty of conductivity while remaining quite thin relative to the ceramic pieces.

When the minimum ejection pressure,  $P_{min}$ , is applied to the piston, the pressure seen by the actuator will be slightly less since the diameter of the actuator is greater than that of the piston. The pressure seen by the actuator,  $P_{stack}$ , when 10 MPa is applied to the piston will be 9.34 MPa.

Next we will calculate the strain of the piezo actuator under the maximum electric field and with the minimum injection pressure applied to the piston,

$$\epsilon_{piezo} = d_{33} * E_{max} - \frac{P_{stack}}{E_{33}} = 7.618 \times 10^{-4}. \quad (2.10)$$

We can now determine the necessary length of piezoelectric material,  $L_{stack}$ , needed in the stack actuator simply by dividing the stroke of the piston by the strain of the piezo material,

$$L_{stack} = \frac{Stroke_{piston}}{\epsilon_{piezo}} = 59.62 \text{ mm}. \quad (2.11)$$

Now that we know how much piezo material is needed, we can determine the integral number of piezo ceramic discs,  $n_{discs}$ , that will be needed to achieve this length,

$$n_{discs} = ceil\left(\frac{L_{stack}}{t_{disc}}\right) = 90 \text{ discs}. \quad (2.12)$$

So the true length of the piezo material in the stack is simply  $n_{discs}$  multiplied by  $t_{disc}$  to give a value,

$$L_{intstack} = n_{discs} * t_{disc} = 60 \text{ mm}. \quad (2.13)$$

The length of the electrode material in the stack,  $L_{electrode}$ , will be,

$$L_{electrode} = (n_{discs} - 1) * t_{electrode} = 8.9 \text{ mm}. \quad (2.14)$$

The full stack actuator length,  $L_{fullstack}$  is then,

$$L_{fullstack} = L_{intstack} + L_{electrode} = 68.9 \text{ mm}. \quad (2.15)$$

#### 2.4.4 Lost Volume

There are two primary sources of lost ejection volume:

1. **Elongation of the steel case** - When the actuator applies the ejection pressure to the fluid the steel case elongates since it is part of the structural loop.

This means that some of the stroke of the actuator is wasted on elongating the steel case rather than ejecting pressurized fluid. We assumed a basic hollow cylindrical shape for the steel casing. The length of the steel casing is slightly longer than the actuator itself. The wall thickness of the steel casing was assigned to be 15 mm. The volume lost due to the elongation of the steel casing is calculated to be 0.733  $\mu\text{L}$ .

2. **Volumetric compression of the fluid** - The fluid itself will compress since in reality it is not perfectly incompressible as is often assumed. At these high pressures the compression of the fluid cannot be ignored,

$$V_{lost} = \frac{V_{fluid} \times P_{min}}{G_{fluid}} = 1.538 \mu\text{L}. \quad (2.16)$$

After accounting for the expected losses, the total volume that will be ejected is 27.73  $\mu\text{L}$ .

### 2.4.5 Resonant Frequency

it is important to calculate the resonant frequency of the stack actuator since this is related to the rise time of the actuator. The rise time is the time required for the stack to fully expand when a step voltage change is applied to the actuator.

The equation for the resonant frequency of a fixed end free end bar is,

$$\omega = \frac{\pi}{2L} \times \sqrt{\frac{E}{\rho}}, \quad (2.17)$$

where  $L$  is the length of the bar,  $E$  is the elastic modulus of the bar, and  $\rho$  is the density of the bar.

Our stack actuator is made up of two materials: the piezoelectric ceramic discs and the metal electrodes in between them. We will assume that the metal electrodes are made of 6061 aluminum.

We will need to calculate the average density and the average elastic modulus of the stack in order to calculate the resonant frequency.

The average density of the bar will be,

$$\rho_{avg} = \frac{\rho_{electrode}L_{electrode} + \rho_{piezo}L_{piezo}}{L_{electrode} + L_{piezo}}. \quad (2.18)$$

Assuming  $\rho_{piezo} = 7.6 \times 10^3 \text{ kg/m}^3$  (the value for PZT) and  $\rho_{electrode} = 2.7 \times 10^3 \text{ kg/m}^3$  (the value for 6061 aluminum) the average density will be  $6.97 \times 10^3 \text{ kg/m}^3$ .

The equation for the equivalent elastic modulus is not so straightforward. We will skip the derivation of the equation and simply present it as,

$$E_{equivalent} = \frac{E_1 E_2 (L_1 + L_2)}{E_1 L_2 + E_2 L_1}, \quad (2.19)$$

where the subscript 1 represents "piezo" and the subscript 2 represents "electrode". The equivalent elastic modulus is calculated to be  $E_{equivalent} = 52.78 \text{ GPa}$ .

We now plug in all these values including the total length of the stack actuator into Equation 2.17. After dividing by  $2\pi$  we arrive at a resonant frequency of 10.0 kHz.

The rise time is known to be approximately one third of the period of the resonance,

$$T_{rise} = \frac{1}{3 * f_{resonance}} = 33.4 \mu s. \quad (2.20)$$

We will see shortly that this is at least 100 times faster than the time involved with the fluid dynamics, which indicates that the ejection will not be limited by the speed of the piezo actuator.

## 2.4.6 Electrical Properties

As an electrical element, piezoelectric ceramics are often modeled using the Butterworth Van Dyke equivalent circuit model shown in Figure 2-8. This circuit model captures both the first resonance and anti-resonance peaks that are characteristic of a piezo element's response to driving input signals of various frequencies. The impedance bode plot that corresponds to this circuit model is shown in Figure 2-9.

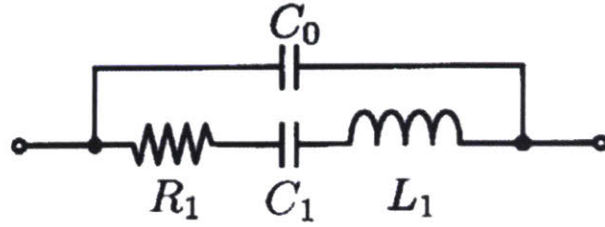


Figure 2-8: Butterworth Van Dyke (BVD) equivalent circuit model for piezoelectric ceramics

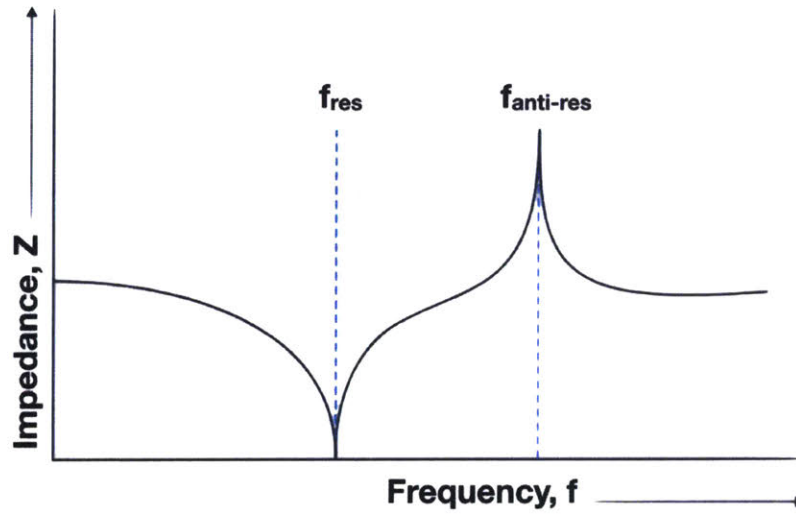


Figure 2-9: Impedance Bode plot for Butterworth Van Dyke (BVD) equivalent circuit model for piezoelectric ceramics. Figure reproduced from [9].

For our purposes, we are most interested in calculating the combined capacitance of  $C_0 + C_1$ . This can be calculated for a single disc element using,

$$C_{disc} = \frac{K_T \cdot \epsilon_0 \cdot A_{disc}}{t_{disc}}, \quad (2.21)$$

where  $K_T$  is the relative dielectric constant and for the 855 material which we are using the value is  $K_T = 3,300$ .  $\epsilon_0$  is the permittivity of free space, which has a value of  $\epsilon_0 = 8.854 \times 10^{-12} \text{ F/m}$ . So the capacitance of each disc in our stack actuator is equal to  $C_{disc} = 0.031 \mu\text{F}$ . And with 90 discs in our stack actuator, the total capacitance is  $C_{stack} = 2.788 \mu\text{F}$ .

Knowing the total stack capacitance we can now calculate the electrical energy stored on the actuator when the full voltage of 1000 V is applied,

$$E_{stack} = \frac{1}{2} \cdot C_{stack} \cdot V_{max}^2 = 1.394 \text{ J}. \quad (2.22)$$

It is useful to know the electrical energy required for each injection. With this value we can determine the power requirements of performing a certain number of injections per second, for example. This would allow one to calculate the necessary DC/DC power conversion requirements in a portable device or calculate the total number of injections that could be completed with a full battery charge.

We are also interested in knowing the electrical current that will be needed to drive our stack actuator. For example, we can calculate what current would be required to fully extend the stack actuator in  $T_{rise}$ , the theoretically fastest actuation time possible,

$$I_{max} = C_{stack} \cdot \frac{V_{max}}{T_{rise}} = 83.5 \text{ A}. \quad (2.23)$$

This value for the maximum driving current that we would ever need will also be useful for designing the electronics that will be driving the stack actuator.

## 2.4.7 First Order Fluid Calculations

Earlier we alluded to the time involved with the fluid ejection itself. A basic way of calculating the approximate value for the ejection time is to use the desired nozzle velocity and nozzle diameter to estimate the average flow rate during ejection. The time it takes for this flow rate to reach the desired injection volume will give us the approximate time scale involved.

We will assume that we are using a nozzle diameter,  $D_{nozzle}$ , of 200  $\mu\text{m}$ . We will further assume that we are achieving a maximum average jet velocity,  $v_{jet}$ , of 200 m/s. Then the ejection time is,



$$T_{ejection} = \frac{V_{inj}}{v_{jet} \cdot A_{nozzle}} = 4.78 \text{ ms}. \quad (2.24)$$

This is indeed over 100 times greater than,  $T_{rise}$ , the rise time of the stack actuator. To be precise it is approximately 143 times greater. This means that our stack actuator will be able to fully compress the fluid before any meaningful amount of the ejection has taken place. This ensures that the dynamics of the system are dominated by the fluid portion of the system rather than the actuator dynamics.

### 2.4.8 Maximum Pressure Achieved

Earlier, in Equation 2.1 we showed how to calculate the theoretical maximum pressure that could be achieved by the piezo stack actuator. We can now fill in the values of the parameters in the equation to calculate  $P_{max}$ . Since we want to calculate the maximum pressure that is applied to the fluid, we also have to adjust for the smaller area of the piston which compresses the fluid relative to the stack area,

$$P_{max} = d_{33} \cdot E_{33} \cdot E_{max} \cdot \frac{A_{stack}}{A_{piston}} = 51.58 \text{ MPa}. \quad (2.25)$$

In reality this will not be the maximum pressure that is applied to the fluid. This equation for  $P_{max}$  assumes that nothing moves or deflects. It assumes that the fluid does not compress, that none of the fluid has yet been ejected from the fluid chamber, that the casing is perfectly rigid, and that the electrode material is perfectly rigid. Of course, none of these assumptions is true and now we want to find out what pressure is actually achieved when we remove some of these idealizations.

We will focus our analysis on four lumped sources of compliance: the compliance of the piezo stack itself including the compliance of the electrodes and the piezo material, the compliance of the liquid in the ejection chamber, the compliance of the preloading element that is used to preload the piezo stack, and the compliance of the steel casing that completes the structural loop. These four lumped compliant elements can be seen in Figure 2-10. This diagram is a simplification of the actuator assembly seen in Figure 2-7.

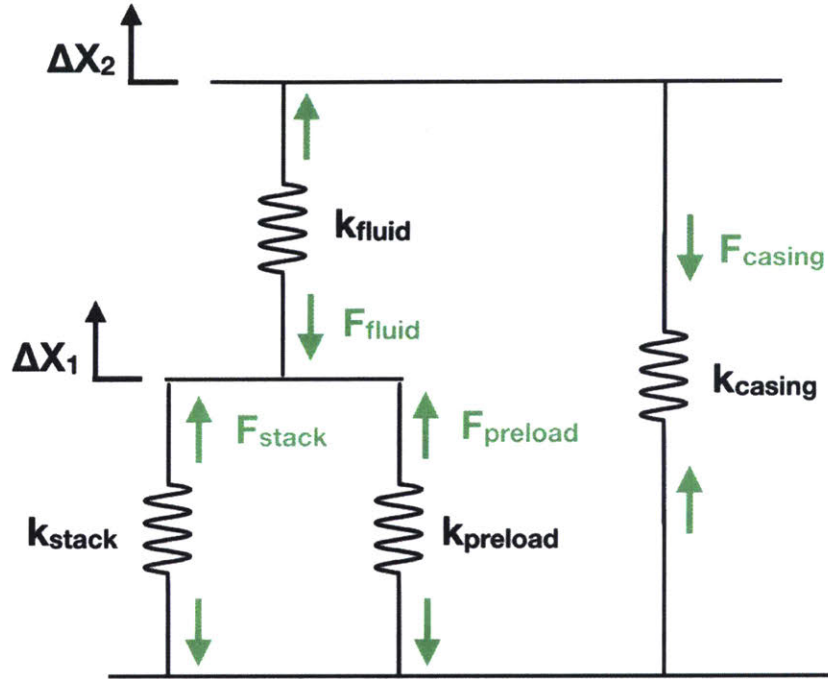


Figure 2-10: Diagram showing the structural loop of the piezo actuator jet injector assembly. This diagram shows the equivalent stiffnesses of the structural members and the important deflections involved. The black arrows show the definition of positive values for  $\Delta X_1$  and  $\Delta X_2$ . The green arrows show the definition of positive forces in each spring equivalent element in the structural loop.

For our analysis of this system, we will assume that the bottom plate in Figure 2-10 remains fixed. We are interested in the movement of the piston relative to the bottom plate and the movement of the top plate relative to the bottom plate. The top plate is the plate which contains the orifice for the fluid jet. The movement of the piston is labeled  $\Delta X_1$ . Both the piezo stack and the preloading element will deflect by  $\Delta X_1$ . The movement of the top plate is labeled  $\Delta X_2$ . The steel casing will extend by  $\Delta X_2$ .

We will now calculate the stiffness values of the elements in Figure 2-10:

$$k_{casing} = \frac{E_{casing} \cdot A_{casing}}{L_{casing}} = 5.95 \cdot 10^9 \text{ N/m}, \quad (2.26)$$

$$k_{stack} = \frac{E_{equivalent} \cdot A_{stack}}{L_{fullstack}} = 5.41 * 10^8 \text{ N/m}, \quad (2.27)$$

$$k_{fluid} = \frac{G_{fluid} \cdot A_{piston}}{t_{fluid}} = 2.84 * 10^9 \text{ N/m}, \quad (2.28)$$

where  $t_{fluid}$  is the thickness of the fluid disc in the ejection chamber.

Since the preloading element is parallel to the piezo stack in the structural loop, it is important that this element have a relatively low stiffness compared with the piezo stack. As the stiffness of the preloading element grows the expansion of the actuator will be less for the same conditions. A common design rule is to keep the stiffness of the preloading element less than or equal to 1/10 the stiffness of the stack actuator. The preloading force should be enough to compress the stack actuator and remove any small air gaps that might be present. For this design we chose a Belville washer to act as the preloading element. The stiffness had a value of  $k_{preload} = 2.23 \times 10^6 \text{ N/m}$ .

The forces in the structural loop are shown in Figure 2-10. The green arrows show the positive definition of these forces in each compliant element. We can now solve the force balance equations below in order to solve for the maximum pressure that is achieved:

$$F_{casing} = k_{casing} \cdot \Delta X_2, \quad (2.29)$$

$$F_{preload} = k_{preload} \cdot (-\Delta X_1), \quad (2.30)$$

$$F_{fluid} = k_{fluid} \cdot (\Delta X_1 - \Delta X_2), \quad (2.31)$$

$$F_{blocking} = d_{33} \cdot E_{max} \cdot E_{33} \cdot A_{stack}, \quad (2.32)$$

$$F_{stack} = F_{blocking} - k_{stack} \cdot \Delta X_1, \quad (2.33)$$

$$F_{casing} = F_{fluid}, \quad (2.34)$$

$$F_{fluid} = F_{stack} + F_{preload}, \quad (2.35)$$

We used a Newton-Raphson numeric solver to solve for all the variables.  $F_{fluid}$

was found to be  $2.66 \times 10^4 N$ . So our maximum fluid pressure is then,

$$P_{realmax} = \frac{F_{fluid}}{A_{piston}} = 40.2 MPa. \quad (2.36)$$

This is over 20% lower than our calculated maximum pressure in Equation 2.25 when we assumed no movement or deflection of the system. It becomes obvious from these equations and from the diagram of the structural loop that we can attain higher pressures that are closer to the theoretical maximum by increasing the stiffness of the casing, increasing the stiffness of the fluid (by decreasing the thickness of the fluid disc), and decreasing the stiffness of the preloading element. In this design, we have already optimized these values to the best achievable levels under our design constraints.

## 2.5 Results of Design Process

We now have a complete stack design that was driven by our original design parameters. The stack actuator consists of 90 piezo discs (made of APC 855 material) that are each 0.667 mm thick and 89 aluminum electrode discs that are 0.1 mm thick. Both the piezo discs and the electrodes have a diameter of 30 mm. The length of the full stack is 68.9 mm. The area of the stack is  $7.069 \times 10^{-4} m^2$ . Figure 2-11 is a picture of a typical stack actuator showing the electrode connections between layers. It is important to note that the poling polarity of the piezo discs in the stack actuator must alternate direction. The electrodes also alternate between a ground electrode and a high voltage electrode throughout the stack. This alternation of disc poling polarity and electrode voltage can be seen in Figure 2-12.

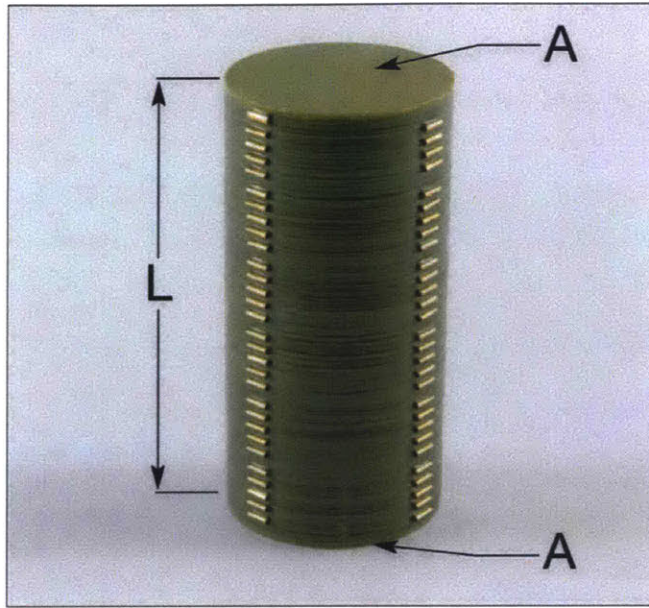


Figure 2-11: Photo of a typical PZT stack actuator after assembly. Image reproduced from [10].

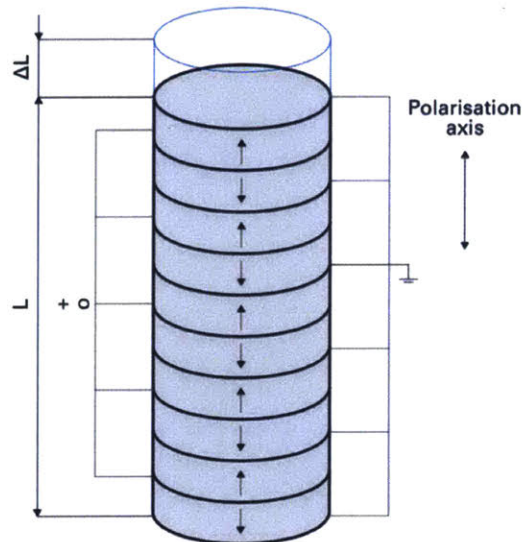


Figure 2-12: Diagram demonstrating the alternation of disc poling polarity and electrode voltage in a stack actuator. Figure reproduced from [9].



# Chapter 3

## Fabrication of Piezoelectric Actuator

### 3.1 Overview of Steps

Basically a list of the steps with a brief description next to each step

1. **Start with lead zirconate titanate (PZT) Powder** - This powder is a proprietary blend of materials mixed with PZT in trace amount to obtain specific properties.
2. **Pressing** - The powder is then pressed using a die and punch into the desired shape for the piezo actuator. The product of this step is called the "green" ceramic
3. **Binder Burn Out** - The green ceramic which has been pressed into a certain shape is put into the furnace to burn out the organic binder material.
4. **Sintering** - The ceramic piece is then put into the furnace in a partially sealed container and brought to a much higher temperature in order to fuse together the grains of ceramic material into one solid ceramic piece.
5. **Disc Slicing** - This step will change depending on the desired geometry. For our purposes the sintered ceramic piece is a rod that then needs to be sliced into thin discs that will be stacked and assembled into the final actuator.

6. **Polishing** - Once the discs are sliced, their surfaces need to be polished in order to remove asperities that will reduce contact area.
7. **Electroding (optional)** - It is sometimes beneficial to add a very thin layer of a conductive material to the two or more surfaces of the ceramic where the voltage will be applied.
8. **Poling** - A high electric field is applied to the ceramic at a high temperature in order to align the crystal domains.
9. **Testing** - The final pieces are tested individually in order to determine their piezoelectric charge constant.

## 3.2 Details of Fabrication Process

### 3.2.1 PZT Powder

We purchased lead zirconate titanate (PZT) powder from APC International, Ltd. As was mentioned earlier in Section 2.3, we chose to use their proprietary 855 soft PZT material. The material powder is pre-reacted, spray-dried hollow spheres of PZT with a range of diameters between 50 and 100  $\mu\text{m}$ .<sup>1</sup> An SEM image of this powder can be seen in Figure 3-1.

The powder also contains an organic binder material. The binder material is often a combination of poly-vinyl alcohol and poly-ethylene glycol. This material acts both as a solid lubricant to allow the grains to flow more freely during pressing as well as a binding material that keeps the pressed green ceramic from breaking during handling in later steps.

---

<sup>1</sup>Note that PZT is especially hazardous in the powdered form since it is much easier to breathe in or consume some by accident. Always work with PZT powder in a fume hood or in a sealed plastic bag that will keep any trace powder from escaping.



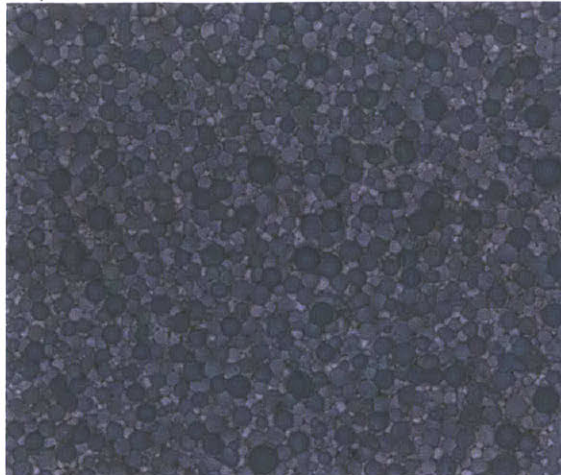


Figure 3-1: PZT Spray-Dried Powder. Image reproduced from [11].

### 3.2.2 Pressing

In order to form the powder into the "green" ceramic pieces, it must be pressed at a high pressure into the desired shape. The recommended pressure for the process is 70 MPa for PZT [11]. We fabricated a die and press for this purpose made out of 306 stainless steel. A picture of the die and press can be seen in Figure 3-2. It is important to leave a gap between the die and press of at least 20  $\mu\text{m}$  so that air can easily escape during the pressing process. We fabricated the die with an inner diameter of 35.57 mm which was calculated in Equation 2.7.

Once the die and press were fabricated we carefully weighed out a known mass of PZT powder (as seen in Figure 3-3) to use for pressing. We pressed the powder in the die and press while using a Devin hydraulic press to apply the necessary 70 MPa pressure. After pressing was complete we used the same hydraulic press to carefully remove the green ceramic rods from the die. The resulting green ceramic rods can be seen in Figure 3-4.

### 3.2.3 Binder Burn Out

The next step is called the binder burnout (BBO) step. The purpose of this step is to burn out the organic binder material that was mixed into the PZT powder to act

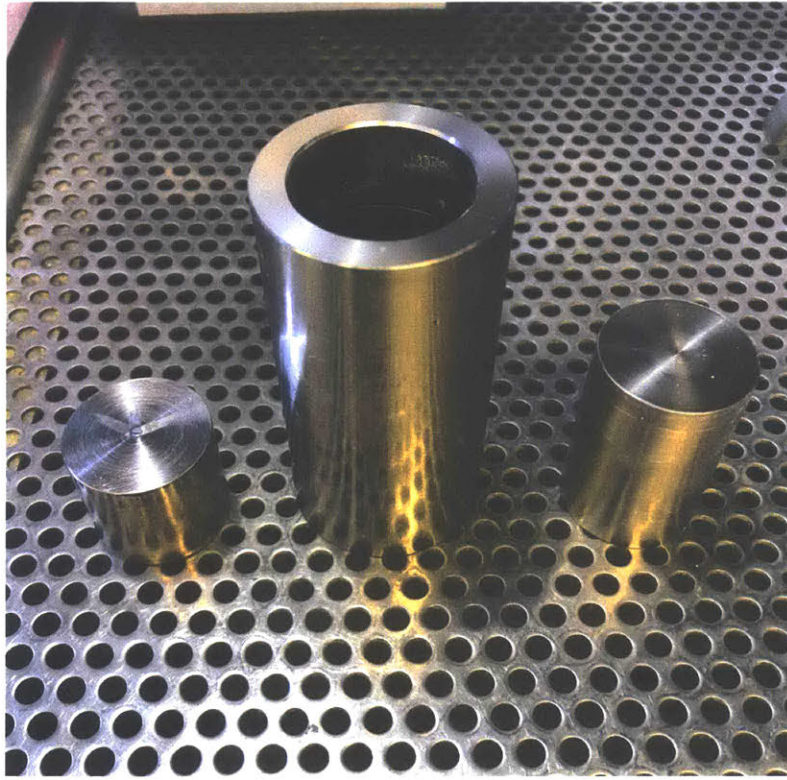


Figure 3-2: Stainless steel punch and die for pressing.

as solid lubricant during pressing and to bind together the green ceramic.

We placed the green ceramic rods into a Thermolyne 47900 furnace on top of a solid sheet of aluminum oxide ceramic. It is important that the rods not be covered and that the furnace be free to vent for this step. This is so that the vapors of the burnt binder material can freely escape. The furnace was programmed to follow the temperature profile shown in Figure 3-5. This profile is designed to dwell at the temperatures at which the majority of the organic binder is being burned away. These temperatures of interest can be determined by performing a thermogravimetric analysis on the PZT powder to see at what temperatures it loses mass most quickly. The maximum temperature of the BBO process was 680 degrees Celsius. The total time for the BBO process was 20 hours. An SEM image of the ceramic after the BBO step is shown in Figure

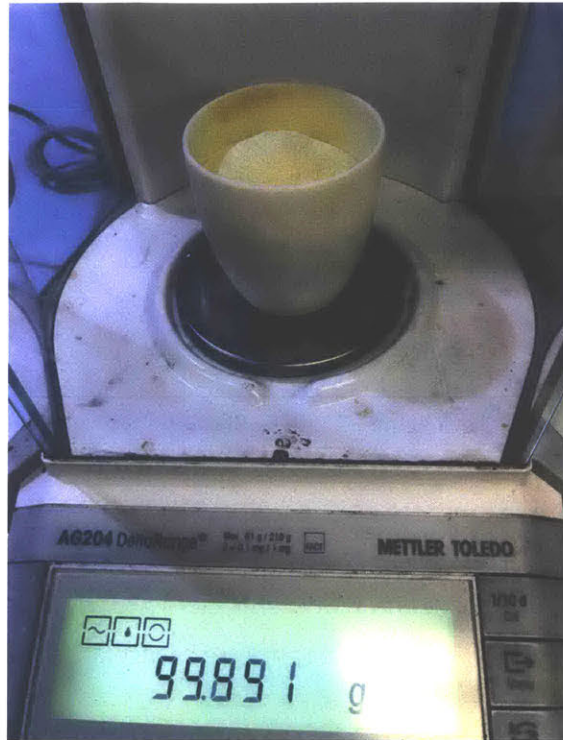


Figure 3-3: Weighing out PZT powder for pressing.

### 3.2.4 Sintering

The sintering step is necessary in order to fuse the ceramic grains together into one solid ceramic piece. This step requires heating the ceramic rods to a temperature of 1200 degrees Celsius inside the furnace and maintaining this temperature for 8 hours.

In this step, the ceramic rods must be placed inside an aluminum oxide vessel that is closed with a lid. It is important that the lid is not sealed so that air is free to escape as the temperature rises. Sealing the lid could lead to the fracture of the aluminum oxide vessel. It is also necessary to put extra PZT powder inside the aluminum oxide vessel for this step. This PZT powder acts as a lead donor material which helps to maintain a partial pressure of lead vapor inside the vessel. Without this partial pressure of lead inside the vessel a significant amount of lead would be lost from the ceramic rods being sintered. The lid helps to keep this lead vapor from escaping the vessel. An image of the aluminum oxide sintering enclosure is seen in Figure 3-7.



Figure 3-4: Green ceramic rods after pressing.

The furnace was programmed to raise the temperature by one degree Celsius per minute until the desired temperature was reached. Once the desired temperature of 1200 degrees Celsius is reached the furnace was programmed to hold this temperature for 8 hours in order to allow sintering to complete. After this period of time the furnace was programmed to bring the temperature back down to ambient temperature at a rate of one degree Celsius per minute. The total time for the sintering procedure was 48 hours. Figure 3-8 shows the rods after sintering is complete.

An SEM image of the ceramic after the sintering step is shown in Figure 3-9. The image reveals that the ceramic grains have now fused into one solid piece of ceramic.

### 3.2.5 Disc Slicing

The sintered ceramic rods now must be sliced into discs of the desired thickness for our stack actuator. Tungsten carbide is not sufficiently hard for cutting PZT and so diamond tooling must be used when machining PZT. We used a sintered diamond saw blade to slice the ceramic rods. The diamond saw blade had a diameter of about 100 mm and a kerf of 0.38 mm. Constant lubrication must be used to cut with this type of saw blade. We performed the disc slicing in a tank of mineral oil that fully

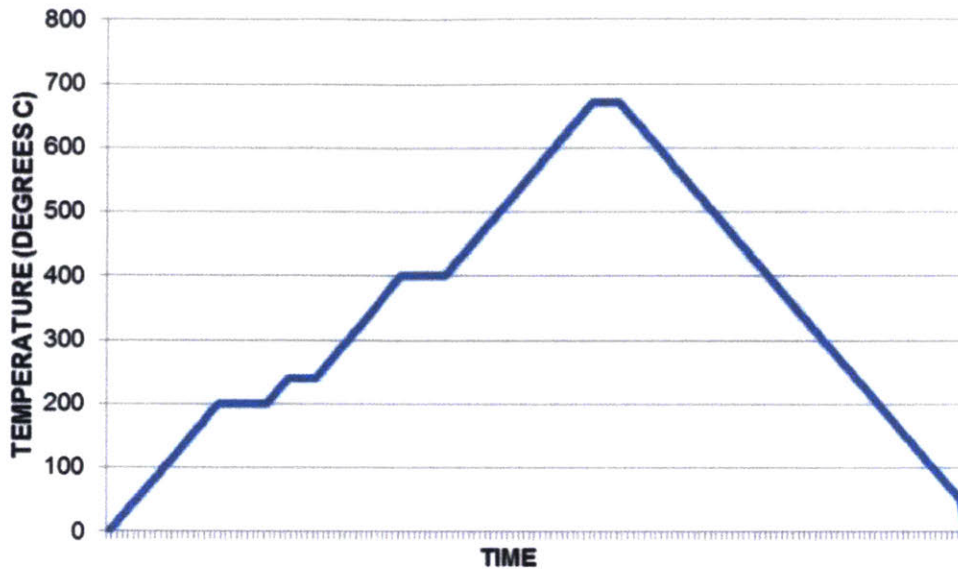


Figure 3-5: Temperature profile for binder burn out step in furnace. The time axis is purposely left blank since the total time can vary. The total time of the process in our case was 20 hours. Figure reproduced from [12].

covered the diamond saw and the PZT rod. Full immersion was necessary to contain the hazardous PZT powder that would be created through the slicing process. Figure 3-10 shows the immersion tank that was used for slicing the PZT discs. We sliced the discs using a spindle speed of 200 RPM and a feed rate of 2 mm/min.

### 3.2.6 Polishing

Once slicing is complete the next step is to polish both sides of these PZT discs. Polishing is necessary in order to achieve a highly flat surface. If the surface finish of the discs is left with a raw, machined finish the stiffness of the interface between the PZT discs and the electrodes will be relatively low. This is because the small asperities that protrude from the unfinished PZT surface first have to be compressed before a larger contact area between the electrodes the PZT discs can be achieved. We used 7 micron diamond polishing sheet in order to polish both sides of each disc to an extremely flat surface finish. An SEM image of the polished disc surface can be seen in Figure 3-11.

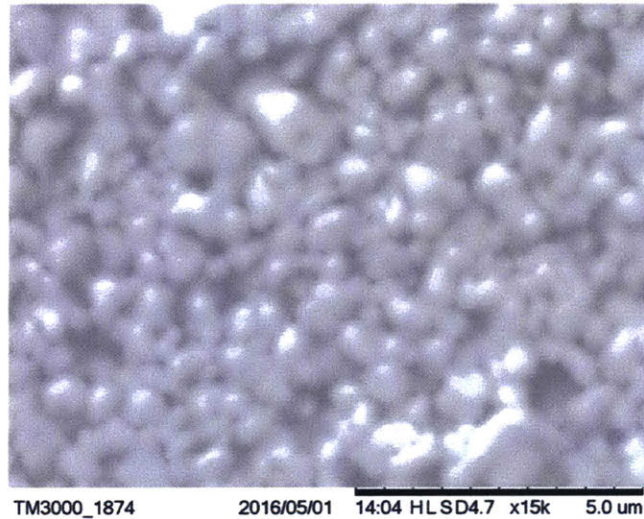


Figure 3-6: SEM image of ceramic after the BBO step. Image taken by Jason Wang.

### 3.2.7 Poling

As we described in Chapter 2, poling is the process used to align all the dipoles of the piezoelectric material in the same direction. The discs are brought to a high temperature just below the Curie temperature and a strong electric field is applied to the discs in order to align the dipoles.

Because we need to apply an electric field of 4 MV/m to the PZT discs, the poling procedure could not be done in air. This is because the necessary electric field for poling is greater than the dielectric strength of air. Arcs would occur in air at a lower electric field and so it would not be possible to reach the necessary electric field for poling. Instead we immersed the discs in mineral oil which could withstand both the high electric field that is needed as well as the high temperature that is needed. The APC 855 material that we used has a Curie temperature of 200 degrees Celsius so we performed our poling procedure at 195 degrees Celsius. The discs were placed between two parallel metal plates supported by a block of PTFE. High voltage wires with silicone conductors were used to conduct the high voltage output of the power supply to the two metal plates that enclosed the PZT discs. We used a Bertan Series 225 high voltage power supply to provide the necessary 2.67 kV. We used an electric fryer with a temperature feedback control system to maintain the mineral oil bath at



Figure 3-7: Sintering Enclosure.

195 degrees Celsius. We applied the poling electric field for 20 minutes to the discs once the temperature had stabilized. Figure 3-12 shows the mineral oil bath with the PTFE block which holds the metal plates and the PZT discs in between.

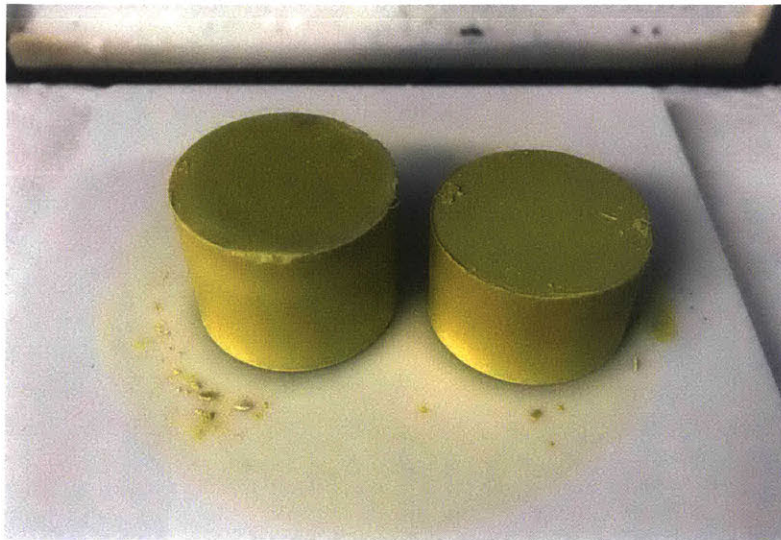
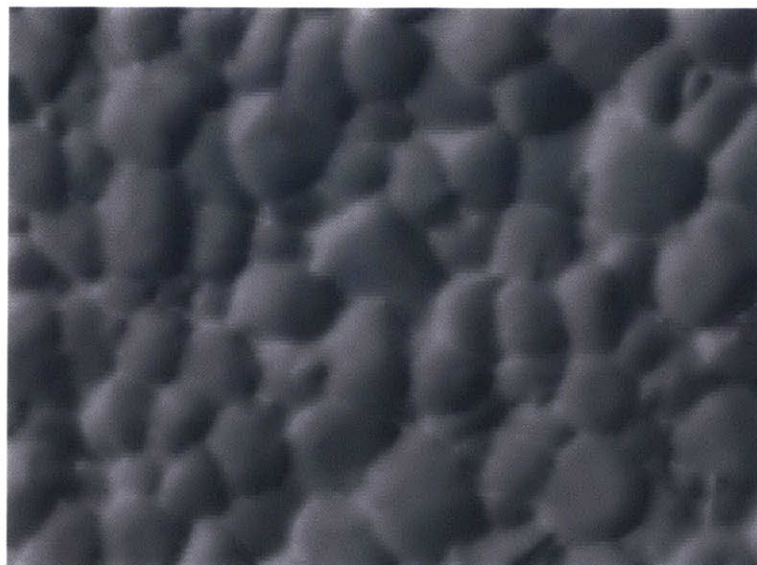


Figure 3-8: Sintered Rods.



TM3000\_1885 2016/05/05 22:01 HLT D5.0 x7.0k 10 um

Figure 3-9: SEM image of sintered PZT ceramic.



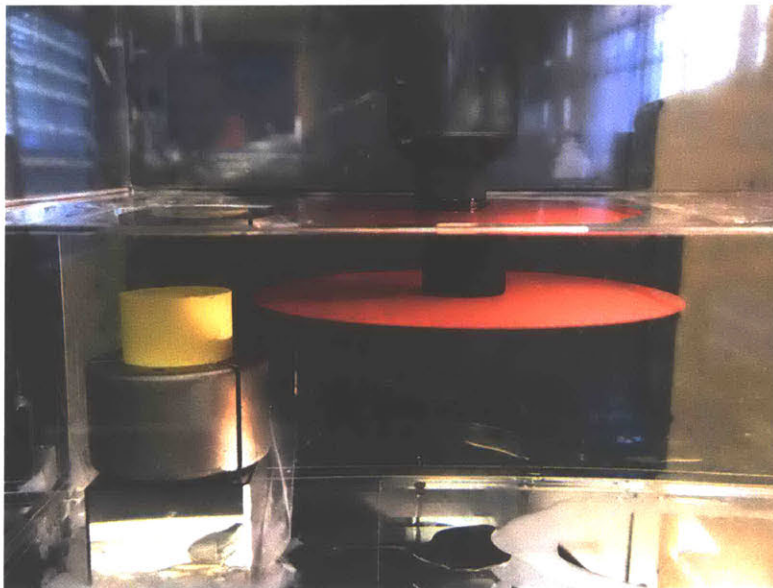
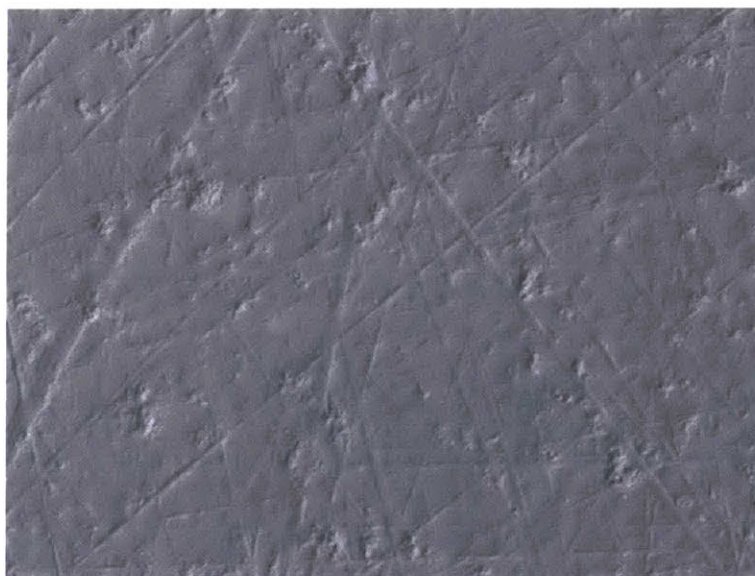


Figure 3-10: Tank with mineral oil for slicing PZT ceramic rod. The sintered diamond saw blade is seen on the right side. The PZT ceramic rod is held in place in a custom machined collet on the left. The holding tank is made of clear acrylic in order to be able to see the process.



TM3000\_1891 2016/05/25 12:14 HLT D4.8 x1.0k 100 um

Figure 3-11: SEM image of polished PZT disc surface.

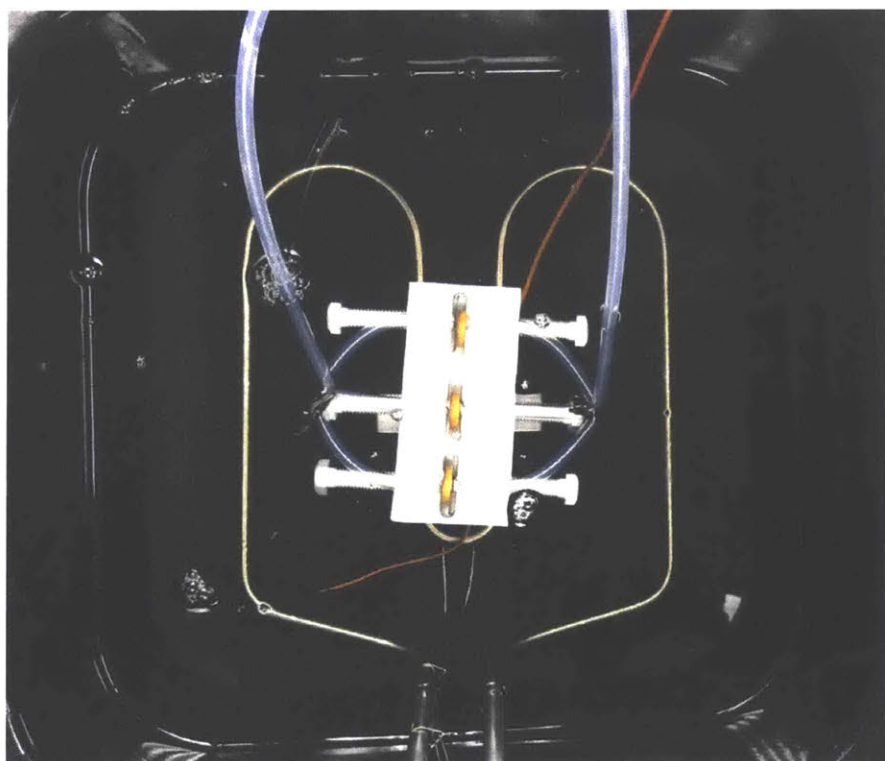


Figure 3-12: Image of the temperature-controlled mineral oil bath used for poling. The white block is made of PTFE and contains the metal plates with the PZT discs in the middle. The high voltage wires with silicone insulation are seen coming from the top to each side.

# Chapter 4

## Experimental Analysis

With all the fabrication steps and poling complete the PZT discs now have their piezoelectric properties and are ready for testing.

### 4.1 Method of Testing Individual Discs

We fabricated one batch of PZT discs using all the steps listed in Chapter 3. From this batch we tested the three PZT discs shown in Figure 4-1. The missing sections seen on the tops of the discs were purposefully cut off using a diamond band saw. This was to remove thicker nubs that were left over from the slicing procedure.

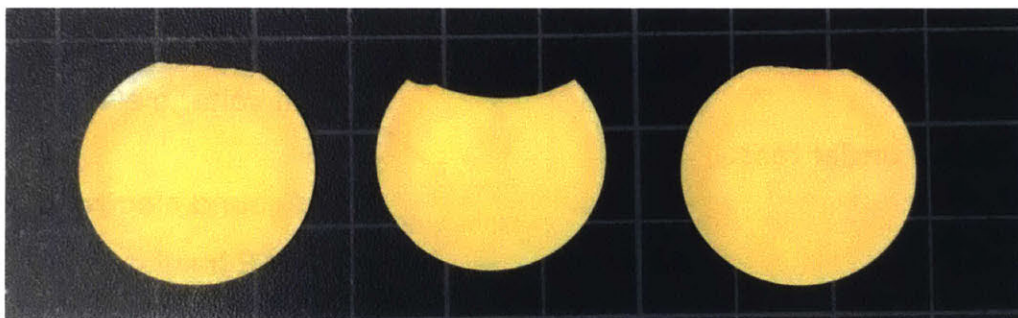


Figure 4-1: Three PZT discs tested.

The experimental setup is shown in Figure 4-2. The PZT discs were placed between two steel plates that acted as the electrodes. A spring clamp applied approximately 15 N of preloading force to compress the PZT disc between the metal plates.

The PZT disc and metal plates were placed on top of a PTFE insulating block to ensure that the high voltage power would be separated from the aluminum fixture. A Keyence laser triangulation distance sensor was used to measure the expansion and contraction of the PZT discs. This sensor has a resolution of 10 nm.

The upper metal plate was connected to the positive output of the Bertan Series 225 high voltage power supply while the lower metal plate was connected to the power supply ground. The upper plate was slowly charged to 1000 V. While 1000 V was applied to the metal plates, 65,000 readings were taken with the Keyence laser distance sensor and averaged to help reduce building vibration noise. Then the voltage was gradually lowered back to zero volts and another 65,000 readings were taken. The difference between these two averages gave the value for one contraction. In this way we measured five expansions and five contractions for each disc.

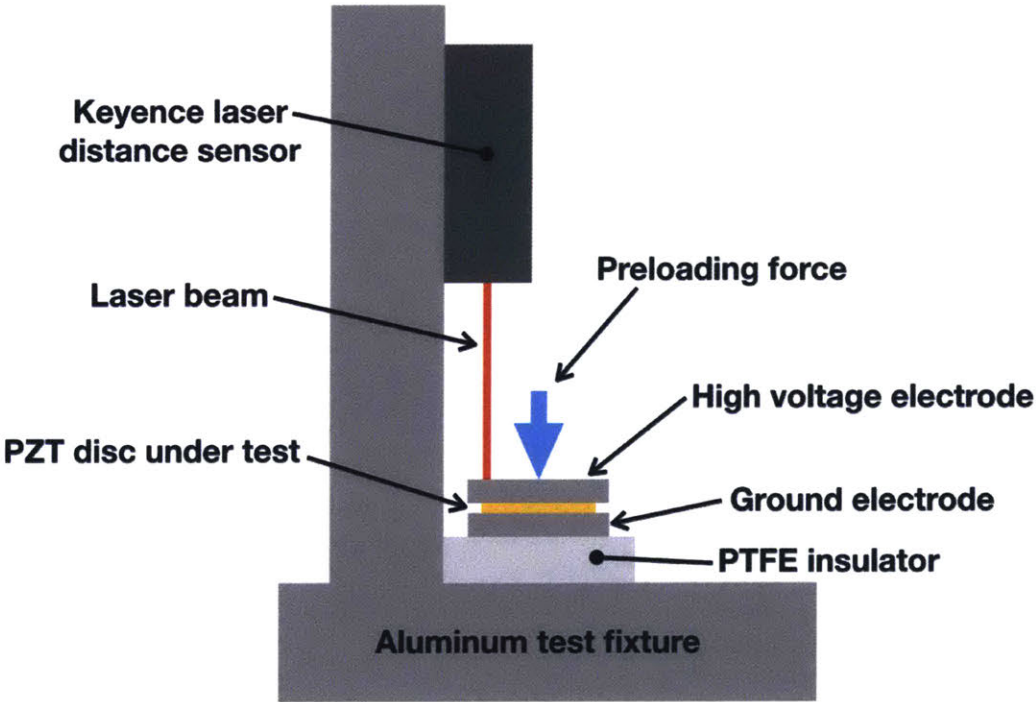


Figure 4-2: Experimental setup for testing disc expansion and contraction.

## 4.2 Results and Discussion

Figure 4-3 shows the average of the 10 expansion/contraction readings taken for each disc and the standard deviation of these values is shown by the error bars. The manufacturer's value of the piezoelectric charge constant for the APC 855 material is  $630 \times 10^{-12} \text{ m/V}$ . The average piezoelectric charge constant for the three discs was measured to be  $509 \pm 66 \times 10^{-12} \text{ m/V}$  which was about 19% lower than the manufacturer's advertised value.

The test results showed conclusively that piezoelectric properties had indeed been imparted to the PZT discs that we fabricated. Our measured value of the average piezoelectric charge constant was approximately 19% lower than the expected value given by the manufacturer. This discrepancy could have been caused by a number of different sources during the fabrication procedure for the discs.

According to the author's belief, the most likely source may have been the irregularity of the electric field that was used during poling. The poling apparatus used thin sheet metal for the electrodes on either side of the PZT discs during poling in the hot mineral oil bath. The thin sheet metal was not perfectly flat and there seemed to be small gaps between the metal surface and the surface of the PZT. Even a relatively small gap of 0.66 mm would have approximately halved the electric field in that region since it would double the distance between the plates. This would cause there to be regions of the PZT discs that would not be as strongly poled as other regions thus diminishing the value of the piezoelectric charge constant.

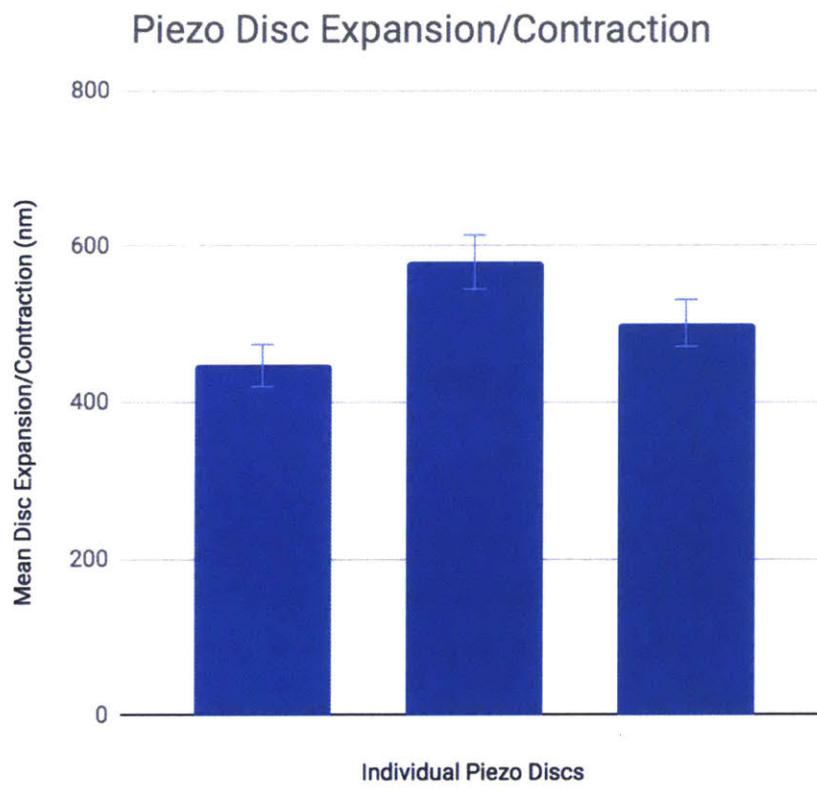


Figure 4-3: Expansion test results.

# Chapter 5

## Conclusion

### 5.1 Future Work

#### 5.1.1 High-Pressure Membrane Design

The diagram in Figure 2-7 shows the moving piston in the assembly that drives the fluid out of the ejection chamber. Of course, it would be necessary to form a seal between the piston and fluid chamber wall in order to avoid losing fluid. Since the volumes of ejection are so small and the pressure of ejection so high with this device even a relatively small compliance in the seal would mean losing ejected volume and a lower pressure. Since the stroke of the piston driven by a piezo stack actuator is on the order of 10 micrometers it is reasonable to instead use a flexure-based seal rather than a sliding seal. Figure 5-1 shows a cross-section of a high-pressure flexure-based seal designed by the author.

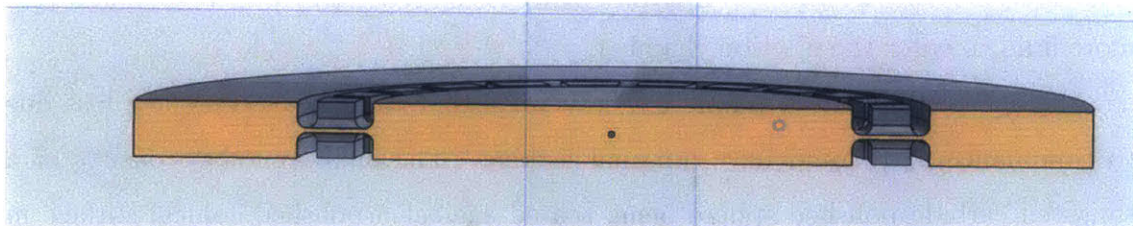


Figure 5-1: High-pressure flexure-based piston seal.

The flexure around the circumference of the center disc allows the center disc to

move by small displacements up and down. The flexure is strengthened by thicker sections which restrict the bellowing motion of the membrane while allowing free movement in the stroke direction of the piston. Figure 5-2 shows results of an FEA analysis on this flexure. This image shows the displacement field of the seal when a pressure is applied to the center disc.

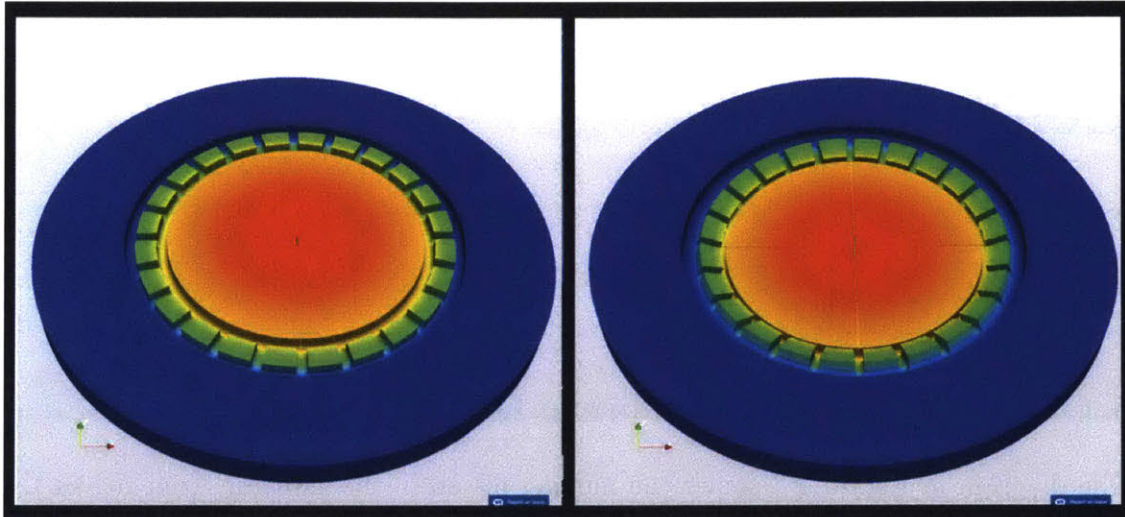


Figure 5-2: Displacement field results of flexure-based seal FEA analysis.

### 5.1.2 High-Pressure Valve Design for Repeated Injections

In order for the stack actuator to be used for multiple low-volume injections in rapid succession it is necessary to have two one-way valves. One one-way would open during actuator expansion and allow fluid to be ejected. During actuator contraction, this first one-way valve would shut and the second one-way valve would open to allow for more fluid to enter the ejection chamber.

The author designed a simple one-way valve that would have very low loss due to compliance and would have minimal leaking. The one-way valve consists of a tungsten carbide polished sphere being seated against a polished conical surface in the stainless steel structure of the ejection chamber. The contact between the sphere and the conical surface is always a circular line regardless of small misalignment. This allows a closed seal to be made using two materials that are inherently very



rigid. Future work might include the building and implementation of this type of high-pressure one-way valve in a repeating injection system.

### **5.1.3 Binary Stochastic System Identification**

Once a full stack actuator is built it would be important to fully characterize the frequency response of the stack actuator. Since high voltages are required to drive the stack actuator it becomes much easier to use binary stochastic system identification rather than swept sine system identification. The author looked into using high voltage power electronics to perform binary stochastic system identification. Specifically silicon carbide field effect transistors (SiCFETs) have both the ability to withstand very high voltage as well as the ability to pass extremely high currents. These latest generation SiCFETs along with a high voltage capacitor bank as the voltage source should function very well when performing binary stochastic system identification on the full stack actuator.

## **5.2 Summary of Conclusions**

This thesis has presented a systematic method for designing a piezoelectric ceramic stack actuator for use with a NFJI device. The presented work is focused on the use of high viscosity and non-newtonian fluids as the delivered fluid with NFJI. The design methodology presented in this thesis can be used in many general cases for designing a piezoelectric stack actuator and the author hopes that it would be useful to other researchers from many different backgrounds. We have also presented an overview of the steps involved with fabricating lead zirconate titanate (PZT) piezoelectric ceramic discs which could be used to build a stack actuator according to our design intention. The author hopes that this work would serve as a useful resource for researchers in the BioInstrumentation Laboratory and elsewhere in the future.



# Appendix A

## High Voltage Safety

High voltage electricity is one of the most dangerous hazards that a researcher can face. It is a silent, invisible killer that kills without warning and kills instantly. Before undertaking any experiment with voltages greater than about 50 V, it is absolutely crucial to study high voltage safety. The following excerpt is reproduced from [13]. Please read this resource carefully!

### **General information about electricity and the human body**

More than one thousand people are killed each year in the U.S. due to generated electric current, and several thousand more are injured. Current flowing inside the body can cause deep burns and cardiac arrest. Frequently, the individual cannot let go of the power source due to involuntary muscle contraction. The brain and heart are the most sensitive organs. For effects of current on the human body, see table 1. An alternating current (ac) with a voltage potential greater than 550 V can puncture the skin and result in immediate contact with the inner body resistance. A 110-V shock may or may not result in a dangerous current, depending on the circuit path, which may include the skin resistance. A shock greater than 600 V will always result in very dangerous current levels. The most severe result of an electrical shock is death. Conditions for

a serious, yet still potentially lethal, shock across a critical path, such as the heart, are

1. More than 30-V root mean square (rms), 42.4-V peak, or 60 V dc at a total impedance of less than 5000 ohms.
2. 10to75mA.
3. More than 10 J.

Conditions for a potentially, but more than likely, lethal shock across the heart are

1. More than 375 V at a total body impedance of less than 5000 ohms.
2. More than 75 mA.
3. More than 50 J.

The worst possible frequency for humans is 60 Hz, which is commonly used in utility power systems. Humans are about five times more sensitive to 60-Hz alternating current than to direct current. At 60 Hz, humans are more than six times as sensitive to alternating current than at 5000 Hz—and the sensitivity appears to decrease still further as the frequency increases. Above 100-200 kHz, sensations change from tingling to warmth, although serious burns can occur from higher radio-frequency energy. At much higher frequencies (e.g., above 1 MHz), the body again becomes sensitive to the effects of an alternating electric current, and contact with a conductor is no longer necessary; energy is transferred to the body by means of electromagnetic radiation.

### **Guidelines for High Voltage Safety**

- Don't work alone - in the event of an emergency another person's presence may be essential.

- Know the emergency procedures to follow in case of an accident (dial 911).
- De-energize the equipment at least twice prior to beginning work. Make sure that the controls applied will prevent operation of the equipment and that all hazardous energy, including residual or stored energy, is blocked, discharged, or relieved prior to starting work.
- After you have discharged everything, only touch the circuit with the back of your hand first. This allows you to let go if you need to.
- Never enter alone into an area containing exposed electrical energy sources.
- Use only the test instruments, and insulated tools rated for the voltage and current specified.
- Always keep one hand in your pocket when anywhere around a powered line-connected or high voltage system.
- Wear rubber bottom shoes or sneakers.
- Don't wear any jewelry or other articles that could accidentally contact circuitry and conduct current, or get caught in moving parts.
- Set up your work area away from possible grounds that you may accidentally contact.
- Know your equipment.
- If you need to probe, solder, or otherwise touch circuits with power off, discharge (across) large power supply filter capacitors (at least 2 times). Monitor while discharging and/or verify that there is no residual charge with a suitable voltmeter.
- If you must probe live, put electrical tape over all but the last 1/16" of the test probes to avoid the possibility of an accidental short, which could cause damage to various components. Clip the reference end of the meter or scope to the appropriate ground return so that you need to only probe

with one hand. Perform as many tests as possible with power off and the equipment unplugged.

- Don't attempt repair work when you are tired. Not only will you be more careless, but also your primary diagnostic tool, deductive reasoning, will not be operating at full capacity.

- Finally, never assume anything without checking it out for yourself! Don't take shortcuts!

# Bibliography

- [1] Anubhav Arora, Itzhak Hakim, Joy Baxter, Ruben Rathnasingham, Ravi Srinivasan, Daniel A Fletcher, and Samir Mitragotri. Needle-free delivery of macromolecules across the skin by nanoliter-volume pulsed microjets. *Proceedings of the National Academy of Sciences*, 104(11):4255–4260, 2007.
- [2] Jeanne C Stachowiak, Marcio G von Muhlen, Thomas H Li, Laleh Jalilian, Sapun H Parekh, and Daniel A Fletcher. Piezoelectric control of needle-free transdermal drug delivery. *Journal of Controlled Release*, 124(1-2):88–97, 2007.
- [3] Jeanne C Stachowiak, Thomas H Li, Anubhav Arora, Samir Mitragotri, and Daniel A Fletcher. Dynamic control of needle-free jet injection. *Journal of Controlled Release*, 135(2):104–112, 2009.
- [4] APC knowledge center: Piezoelectricity. <https://www.americanpiezo.com/knowledge-center/piezo-theory/piezoelectricity.html>.
- [5] Wikipedia: Lead zirconate titanate. [https://en.wikipedia.org/wiki/Lead\\_zirconate\\_titanate](https://en.wikipedia.org/wiki/Lead_zirconate_titanate).
- [6] Center for industrial rheology: Rheological profile of hyaluronic acid solutions and gels. <http://www.rheologylab.com/articles/pharma/rheological-profile-hyaluronic-acid/>.
- [7] APC International Ltd. *Piezoelectric Ceramics: Principles and Applications*. APC International, 2011.
- [8] PI: Basic designs of piezoelectric positioning elements: Piezo stacks and tubes. [http://www.pi-usa.us/tutorial/4\\_39.html](http://www.pi-usa.us/tutorial/4_39.html).
- [9] PI: Fundamentals of piezo technology. <https://www.physikinstrumente.com/en/technology/piezo-technology/fundamentals/>.
- [10] APC International Ltd. *First Steps Towards Piezoaction*. APC International.
- [11] APC: Ceramic manufacturing series of pressing pzt powders. <https://www.americanpiezo.com/blog/ceramic-manufacturing-series-pressing-pzt-powders/>.

- [12] APC: Ceramic manufacturing series firing pressed pzt components. <https://www.americanpiezo.com/blog/ceramic-manufacturing-series-firing-pressed-pzt-components/>.
- [13] Colorado state university high voltage safety manual. [http://projects-web.engr.colostate.edu/ece-sr-design/AY13/measurement/High\\_Voltage\\_Safety\\_Manual.pdf](http://projects-web.engr.colostate.edu/ece-sr-design/AY13/measurement/High_Voltage_Safety_Manual.pdf).